Sagittal Plane Waves in Infinitely Periodic Multilayered Composites Composed of Alternating Viscoelastic and Elastic Solids

A. B. M. Tahidul Haque
Department of Civil, Structural and Environmental Engineering,
University at Buffalo,
Buffalo, NY 14260

Ratiba F. Ghachi
Department of Civil and Architectural Engineering,
Qatar University,
P. O. Box 2713,
Doha, Qatar

Wael I. Alnahhal
Department of Civil and Architectural Engineering,
Qatar University
P. O. Box 2713,
Doha, Qatar

Amjad Aref
Department of Civil, Structural and Environmental Engineering,
University at Buffalo,
Buffalo, NY 14260

Jongmin Shim[1]
Department of Civil, Structural and Environmental Engineering,
University at Buffalo,
240 Ketter Hall,
Buffalo, NY 14260
e-mail: jshim@buffalo.edu

In order to design phononic crystals whose band-gaps are located in low-frequency ranges, researchers commonly adopt low stiffness polymeric materials as key constituents and exploit the high impedance mismatch between metals and polymers. However, there has been very little research on wave propagation at arbitrary angles in the sagittal plane of viscoelastic-elastic multilayered composites because there exist the intricate wave attenuation characteristics at the layer interfaces. The objective of our investigation is to obtain analytical dispersion relation for oblique wave motion in the sagittal plane of infinitely periodic multilayered composite composed of alternating viscoelastic and elastic solids, where the attenuation of harmonic plane waves is found to occur only in the direction perpendicular to the layers. By using this wave propagation characteristic, we directly apply the semi-analytical approach employed in elastic multilayered composites to calculate the dispersion relation of sagittal plane waves in alternating viscoelastic-elastic multilayered composites. Specifically, we consider a bilayered composite composed of alternating aluminum and polyurethane elastomer, whose complex-valued viscoelastic moduli are experimentally determined by performing dynamic mechanical analysis (DMA). The analysis shows that the alternating viscoelastic-elastic layered composite does not possess a phononic band-gap regardless of incident angles. In addition, wave motions at oblique angles are found to travel with a wide range of frequency contents compared to wave motions perpendicular to the layers. The presented analysis demonstrates that wave dispersion relation in viscoelastic-elastic layered composites is distinctly different from the corresponding elastic counterpart, and highlights the importance of the viscoelastic modeling of polymeric materials in wave dispersion analysis.
[DOI: 10.1115/1.4039039]

1 Introduction

Elastic layered composites possess interesting wave characteristics, so that they have been employed in numerous dynamic applications such as phononic band-gaps [1–8], negative effective dynamic properties [9,10], tunable piezoelectric materials [11], controllable thermal conductivity [12,13], acoustic rectifier [14,15], and acoustic waveguide [16]. The intriguing applications are mostly attributed to their particular phononic dispersion relation, which has been extensively investigated. The dispersion relations of elastic layered composites have been analytically calculated for waves perpendicular to the layers [17–20]. For sagittal plane waves at arbitrary directions, researchers have also obtained the semi-analytical dispersion relations of elastic layered composites [21–28]. Note that sagittal plane waves refer to the coupled P-wave (pressure wave) and SV-wave (shear vertical wave) [29–32], and Fig. 1 illustrates oblique angles in the sagittal plane (i.e., $x_1 - x_2$ plane).

Elastic layered composites composed of metals show unique wave characteristics typically at high frequency ranges (e.g., MHz or higher), but unwanted vibrations and noises disturbing human body are characterized by low frequency ranges (e.g., a few kHz or lower) [33–35]. In order to bring down the available frequency range of layered composites to practical ranges, researchers commonly choose polymeric materials as one constituent of composites and exploit the high impedance mismatch between metals and polymers. Since experimental studies [36,37] showed that the viscoelastic behavior of polymers affects the wave transmission characteristics of layered composites, a group of researchers have considered the viscoelasticity of polymers to study the wave characteristics. However, studies investigating the comprehensive dispersion relation (i.e., frequency-wavenumber relation) of *infinitely periodic layered composites* have been limited for wave propagation perpendicular to the layers [38–42]. For example, using frequency-dependent complex moduli, Tanaka and Kon-No analytically studied the dispersion relations of waves perpendicular to the layers in infinitely periodic layered composites composed of viscoelastic and elastic solids (i.e., viscoelastic-elastic layered composites) [38]. Similar studies have also been performed using several numerical techniques, including finite difference method [39], variational method [40], Fourier expansion method [41], and plane wave expansion method [42].

It is also a noteworthy fact that another group of researchers has intensively studied the transmission and reflection of *oblique wave motion* in viscoelastic medium by addressing the intricate wave attenuation characteristics at the viscoelastic layer interfaces [43–52]. However, the effect of attenuation angle is studied only for finite multilayered composites, where Bloch theorem is not applied, so the complete dispersion relation cannot be obtained. For instance, Borcherdt [45] has investigated mainly horizontal wave (i.e., SH-wave) and Love surface wave in finite viscoelastic

[1]Corresponding author.

Contributed by the Applied Mechanics Division of ASME for publication in the Journal of Applied Mechanics. Manuscript received September 8, 2017; final manuscript received January 16, 2018; published online February 2, 2018. Editor: Yonggang Huang.

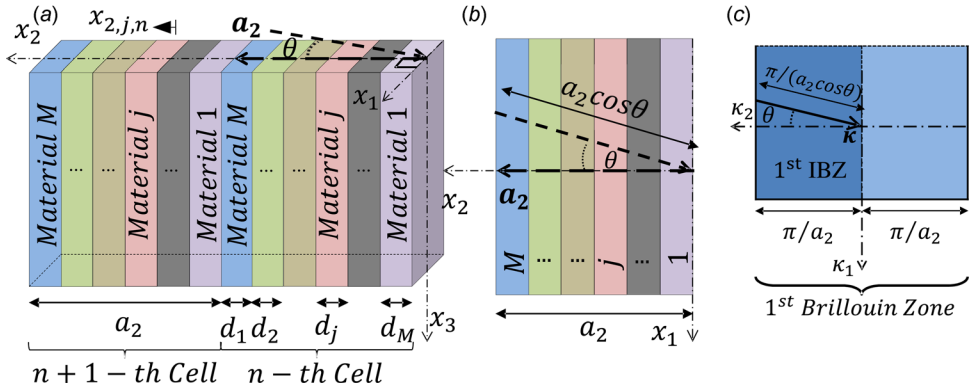

Fig. 1 (*a*) Infinitely periodic *M*-layered composite that is periodic along the x_2-axis. The primitive lattice vector $\mathbf{a}_2$ defines the unit cell of the composite with a periodic length $a_2 = ||\mathbf{a}_2||$. (*b*) Unit cell of the *M*-layered composite in the two-dimensional (2D) sagittal plane where wave can propagate in any direction by making angle θ with the x_2-axis. The periodic length of the inclined wave is given by $(a_2 \cos\theta)$. (*c*) Reciprocal space of the *M*-layered composite showing the first Brillouin zone on the $\kappa_1-\kappa_2$ plane. The rectangle on the right represents the IBZ which is bounded by $\kappa_2 \in [0, \pi/a_2]$ in the κ_2-axis. The propagating wavevector κ describes wave motion at an angle θ which has periodic length $\pi/(a_2 \cos\theta)$ in the reciprocal space.

multilayered composites. Moreover, other researchers have studied only the transmission and reflection of waves in finite viscoelastic-elastic layered composites [46,47,52], which have not included the comprehensive dispersion relation.

The objective of our investigation is to obtain analytical dispersion relation for oblique wave motion in the sagittal plane of infinitely periodic multilayered composite composed of alternating viscoelastic and elastic solids. In this study, we integrate the above two groups' approaches to wave motion. So, the attenuation characteristics studied in the wave transmission and reflection at viscoelastic interfaces are adopted to analytically study the dispersion relation of viscoelastic-elastic infinitely periodic multilayered composites. The direction of wave attenuation in viscoelastic solids is generally found to be different from the direction of wave propagation [47,53]. We first address the challenges of the sagittal plane wave analysis in an arbitrary viscoelastic layered composite and then focus on a class of infinitely periodic layered composites composed of *alternating* viscoelastic and elastic solids (i.e., alternating viscoelastic-elastic layered composites). Note that the attenuation of harmonic plane waves occurs only in the direction perpendicular to the layers in alternating viscoelastic-elastic multilayered composites [46,47,52]. Using this wave propagation characteristic, we directly apply the semi-analytical approach employed in elastic multilayered composites to find the dispersion relation of sagittal plane waves in alternating viscoelastic-elastic multilayered composites. Then, the dispersion relation of an alternating viscoelastic-elastic layered composite is compared with its elastic counterpart to illustrate the distinct effects of viscoelastic properties. Furthermore, we present the transmission coefficient and the group slowness, which efficiently illustrate the viscoelastic effects on wave motions at various directions in the sagittal plane. Section 2 reviews the analytical fundamentals and derives the semi-analytical dispersion relation of the infinitely periodic multilayered composites composed of alternating viscoelastic and elastic solids. In Sec. 3, the derived semi-analytical solution is adopted to calculate the dispersion relation of a specific bilayered composite composed of alternating aluminum and polyurethane elastomer. Discussion and conclusion are presented in Secs. 4 and 5, respectively.

2 Analysis

This section starts with a brief review of wave motions in isotropic viscoelastic solids. Then, we revisit the generalized elastodynamic Snell's law by considering two semi-infinite viscoelastic solids in contact and specialize it for viscoelastic-elastic interfaces. The outcome of the specialized case for viscoelastic-elastic interfaces is applied to investigate sagittal plane waves in alternating viscoelastic-elastic multilayered composites.

2.1 Waves in Isotropic Viscoelastic Solids. Due to material damping, wave propagation characteristics in viscoelastic solids deviate from ones in elastic solids in many aspects [54,55]. In particular, the constitutive relation for a linear viscoelastic material is often expressed in the form of the hereditary integral [56]. In the absence of the body force, the equations for a homogeneous isotropic viscoelastic solid can be summarized as

$$\begin{aligned} \nabla \cdot \boldsymbol{\sigma}(\mathbf{x},t) &= \rho \ddot{\mathbf{u}}(\mathbf{x},t), \\ \boldsymbol{\varepsilon}(\mathbf{x},t) &= \frac{1}{2}\left[\nabla \mathbf{u}(\mathbf{x},t) + \nabla \mathbf{u}(\mathbf{x},t)^{\mathrm{T}}\right], \\ \boldsymbol{\sigma}(\mathbf{x},t) &= \int_{-\infty}^{\infty} \left[\lambda(t-\tau)\,\mathrm{tr}\left[\dot{\boldsymbol{\varepsilon}}(\mathbf{x},\tau)\right]\mathbf{1} + 2\,\mu(t-\tau)\dot{\boldsymbol{\varepsilon}}\,(\mathbf{x},\tau)\right] d\tau \end{aligned} \tag{1}$$

where $\mathbf{u}(\mathbf{x},t)$ is the displacement field at the position $\mathbf{x}$ and time t, $\boldsymbol{\sigma}$ is the stress tensor, $\boldsymbol{\varepsilon}$ is the strain tensor, 1 is the second-order identity tensor, ∇ is the nabla operator, tr $\square$ denotes the trace, ρ is the constant mass density, and λ and μ are the relaxation moduli [57]. Note that the causality requires $\lambda(t-\tau) = \mu(t-\tau) = 0$ for $\tau > t$ in Eq. $(1)_3$.

Now, we consider a harmonic wave motion characterized by an angular frequency ω

$$\mathbf{u}(\mathbf{x},t) = \bar{\mathbf{u}}(\mathbf{x})e^{i\omega t}, \quad \boldsymbol{\sigma}(\mathbf{x},t) = \bar{\boldsymbol{\sigma}}(\mathbf{x})e^{i\omega t}, \quad \boldsymbol{\varepsilon}(\mathbf{x},t) = \bar{\boldsymbol{\varepsilon}}(\mathbf{x})e^{i\omega t} \tag{2}$$

where $i = \sqrt{-1}$ and the overbar $\bar{\square}$ indicates the position-dependent amplitude. Then, the substitution of Eq. (2) into Eq. (1) provides the governing equation for the displacement field

$$\left[\hat{\lambda}(\omega) + 2\hat{\mu}(\omega)\right]\nabla[\nabla \cdot \bar{\mathbf{u}}(\mathbf{x})] - \hat{\mu}(\omega)\nabla \times \nabla \times \bar{\mathbf{u}}(\mathbf{x}) + \omega^2 \rho \bar{\mathbf{u}}(\mathbf{x}) = 0 \tag{3}$$

where $\hat{\lambda}(\omega) = i\,\omega \int_{-\infty}^{\infty} \lambda(t) e^{-i\omega t} dt$ and $\hat{\mu}(\omega) = i\,\omega \int_{-\infty}^{\infty} \mu(t) e^{-i\omega t} dt$ are the complex viscoelastic moduli [58,59]. Subsequently, Helmholtz's theorem [45] can be applied to decompose the displacement field into the sum of a curl-free vector field and a divergence-free vector field using a dilatation-related scalar potential $\bar{\Phi}(\mathbf{x})$ and a rotation-related vector potential $\bar{\mathbf{H}}(\mathbf{x})$

$= [\bar{H}_1\, \bar{H}_2\, \bar{H}_3]^{\mathrm{T}}$, i.e., $\bar{\mathbf{u}}(\mathbf{x}) = \nabla\bar{\Phi}(\mathbf{x}) + \nabla \times \bar{\mathbf{H}}(\mathbf{x})$ with $\nabla \cdot \bar{\mathbf{H}}(\mathbf{x}) = 0$. Then, Eq. (3) becomes two decoupled governing equations

$$\begin{aligned} \left[\hat{\lambda}(\omega) + 2\,\hat{\mu}(\omega)\right] \nabla^2\bar{\Phi}(\mathbf{x}) + \omega^2\rho\,\bar{\Phi}(\mathbf{x}) = 0, \\ \hat{\mu}(\omega)\,\nabla^2\bar{\mathbf{H}}(\mathbf{x}) + \omega^2\rho\,\bar{\mathbf{H}}(\mathbf{x}) = 0 \end{aligned} \tag{4}$$

where the first equation governs the wave motion of dilatation-related disturbance, whereas the second one governs the rotational wave propagation in viscoelastic solids. From the above equations, the dilatational wave velocity c_p and the rotational wave velocity c_s are defined by

$$c_p(\omega) = \sqrt{\frac{\hat{\lambda}(\omega) + 2\,\hat{\mu}(\omega)}{\rho}}, \quad c_s(\omega) = \sqrt{\frac{\hat{\mu}(\omega)}{\rho}} \tag{5}$$

where the subscripts p and s indicate the pressure (i.e., longitudinal or dilatational) and the shear (i.e., transverse or rotational) waves, respectively. These complex-valued wave velocities imply that plane waves in viscoelastic solids are dispersive and attenuating [58,60].

Furthermore, we consider a plane wave characterized by a complex wavevector $\boldsymbol{\kappa}$

$$\bar{\mathbf{u}}(\mathbf{x}) = \breve{\mathbf{u}}\, e^{i\boldsymbol{\kappa}\cdot\mathbf{x}} = \breve{\mathbf{u}}\, e^{i\kappa\mathbf{n}\cdot\mathbf{x}} \tag{6}$$

where $\breve{\mathbf{u}}$ is the displacement amplitude along the wave plane, κ is the wavenumber, and $\mathbf{n}$ is the vector indicating the direction of the plane wave. The condition for the plane wave to satisfy the governing equation (3) results in the following eigenvalue problem:

$$\frac{1}{\rho\omega^2}\left[\left[\hat{\lambda}(\omega) + 2\hat{\mu}(\omega)\right]\mathbf{n}\otimes\mathbf{n} + \hat{\mu}(\omega)\mathbf{1}\right]\cdot\breve{\mathbf{u}} = \frac{1}{\kappa^2}\breve{\mathbf{u}} \tag{7}$$

where $\otimes$ denotes the tensor product. In order to obtain a nontrivial wave motion $\bar{\mathbf{u}}(\mathbf{x})$, we eventually obtain two sets of complex-valued eigenvalues κ and eigenvectors $\breve{\mathbf{u}}$

$$\kappa_p(\omega) = \frac{\omega}{c_p(\omega)} = \sqrt{\frac{\rho\omega^2}{\hat{\lambda}(\omega) + 2\hat{\mu}(\omega)}}, \quad \kappa_s(\omega) = \frac{\omega}{c_s(\omega)} = \sqrt{\frac{\rho\omega^2}{\hat{\mu}\,(\omega)}} \tag{8}$$

$$\breve{\mathbf{u}}_p = \mathbf{n}, \quad \breve{\mathbf{u}}_s = \mathbf{m} \quad \text{with} \quad \mathbf{m}\cdot\mathbf{n} = 0 \tag{9}$$

which implies that the particle displacement of the pressure wave is parallel to the direction of the wave propagation, whereas the particle displacement of the shear wave is perpendicular to the direction of the wave propagation. Here, the eigenvalues $\kappa_p(\omega)$ and $\kappa_s(\omega)$ can also be viewed as viscoelastic material properties derived from the complex viscoelastic moduli $\hat{\lambda}(\omega)$ and $\hat{\mu}(\omega)$.

In general, wave propagation and wave attenuation can be described by using a complex-valued wavevector $\boldsymbol{\kappa}$, which is expressed by [47,52]

$$\boldsymbol{\kappa} = \boldsymbol{\kappa}^R + i\,\boldsymbol{\kappa}^I = \hat{\kappa}^R\mathbf{n}^R + i\,\hat{\kappa}^I\mathbf{n}^I \tag{10}$$

where the quantities denoted by the superscripts R and I are real-valued; $\mathbf{n}^Q = \boldsymbol{\kappa}^Q/||\boldsymbol{\kappa}^Q||$ for $Q = R, I$ with $||\square||$ denoting the Euclidean norm; and the over-hat $\hat{\square}$ indicates the real-valued magnitude with respect to the corresponding wavevector. Note that $\mathbf{n}^R$ and $\mathbf{n}^I$ indicate the directions of wave propagation and wave attenuation, respectively. In addition, $\hat{\kappa}^R$ describes the phase of wave propagation, while $\hat{\kappa}^I$ is relating to the amplitude of wave attenuation.

2.2 Plane Waves in Two Semi-Infinite Viscoelastic Solids in Contact. Many researchers have investigated the oblique incidences of waves at viscoelastic interfaces (i.e., interface between two viscoelastic solids) [49,51,61,62] as well as at viscoelastic-elastic interfaces (i.e., interface shared by elastic and viscoelastic solids) [46,47]. This subsection briefly reviews the generalized elastodynamic Snell's law at viscoelastic interfaces. Then, Snell's law is applied to viscoelastic-elastic interfaces, which are encountered in the periodic multilayered composites composed of alternating viscoelastic and elastic solids, i.e., the focus of this study.

When a propagating plane wave encounters an interface between two viscoelastic solids, both refracted and reflected waves occur. It is also well known that the direction of wave attenuation in viscoelastic solids is generally different from the direction of wave propagation [47,53]. We consider two viscoelastic layers, which are in contact along the plane $x_2 = 0$ as shown in Fig. 2. Then, the propagation angle θ and the attenuation angle ζ for each layer can be represented by [47]

$$\theta_{r,j} = \cos^{-1}\left(\mathbf{n}^R_{r,j}\cdot\mathbf{e}_2\right), \quad \zeta_{r,j} = \cos^{-1}\left(\mathbf{n}^I_{r,j}\cdot\mathbf{n}^R_{r,j}\right), \quad \text{for} \quad r = p, s \quad \text{and} \quad j = 1, 2 \tag{11}$$

The attenuation angle ζ is a unique wave characteristic of a viscoelastic solid, and it is known to be dependent on the homogeneity of a viscoelastic solid [63]. While a homogeneous plane wave is characterized by $\zeta = 0$, a wave with a nonzero value of ζ is referred to as an inhomogeneous plane wave. For a plane wave encountering the considered viscoelastic layer interface, the governing equations in Eq. (4) resolve wave motion into two decoupled parts: anti-plane shear waves (i.e., SH-wave) and sagittal plane waves (i.e., P- and SV-waves, which are the main concern of this study). The wave motion of sagittal plane waves for the j-th layer ($j = 1, 2$) is governed by

$$\begin{aligned} \nabla^2\bar{\Phi}_j(\mathbf{x}) + \kappa^2_{p,j}(\omega)\,\bar{\Phi}_j(\mathbf{x}) = 0, \\ \nabla^2\bar{H}_{3,j}(\mathbf{x}) + \kappa^2_{s,j}(\omega)\,\bar{H}_{3,j}(\mathbf{x}) = 0, \end{aligned} \quad \text{for} \quad j = 1, 2 \tag{12}$$

Subsequently, the general solution can be easily obtained by

$$\begin{aligned} \bar{\Phi}_j(\mathbf{x}) &= \bar{\phi}_{F,j}\, e^{i\left(\hat{\kappa}^R_{p,j}\mathbf{n}^R_{p,F,j} + i\hat{\kappa}^I_{p,j}\mathbf{n}^I_{p,F,j}\right)\cdot\mathbf{x}} + \bar{\phi}_{B,j}\, e^{i\left(\hat{\kappa}^R_{p,j}\mathbf{n}^R_{p,B,j} + i\hat{\kappa}^I_{p,j}\mathbf{n}^I_{p,B,j}\right)\cdot\mathbf{x}}, \\ \bar{H}_{3,j}(\mathbf{x}) &= \bar{h}_{F,j}\, e^{i\left(\hat{\kappa}^R_{s,j}\mathbf{n}^R_{s,F,j} + i\hat{\kappa}^I_{s,j}\mathbf{n}^I_{s,F,j}\right)\cdot\mathbf{x}} + \bar{h}_{B,j}\, e^{i\left(\hat{\kappa}^R_{s,j}\mathbf{n}^R_{s,B,j} + i\hat{\kappa}^I_{s,j}\mathbf{n}^I_{s,B,j}\right)\cdot\mathbf{x}}, \end{aligned} \quad \text{for} \quad j = 1, 2 \tag{13}$$

where $\bar{\phi}_{F,j}$, $\bar{\phi}_{B,j}$, $\bar{h}_{F,j}$, and $\bar{h}_{B,j}$ are potential amplitudes to be determined from boundary conditions at the viscoelastic layer interface; and

$$\begin{aligned} \mathbf{n}^R_{r,F,j} &= \begin{bmatrix} \sin\theta_{r,j} \\ -\cos\theta_{r,j} \end{bmatrix}, \quad \mathbf{n}^I_{r,F,j} = \begin{bmatrix} \sin\left(\theta_{r,j} + \zeta_{r,j}\right) \\ -\cos\left(\theta_{r,j} + \zeta_{r,j}\right) \end{bmatrix}, \\ \mathbf{n}^R_{r,B,j} &= \begin{bmatrix} \sin\theta_{r,j} \\ \cos\theta_{r,j} \end{bmatrix}, \quad \mathbf{n}^I_{r,B,j} = \begin{bmatrix} \sin\left(\theta_{r,j} + \zeta_{r,j}\right) \\ \cos\left(\theta_{r,j} + \zeta_{r,j}\right) \end{bmatrix}, \end{aligned} \quad \text{for} \quad r = p, s \tag{14}$$

By substituting the general solution for $\bar{\Phi}_j$ and $\bar{H}_{3,j}$ into Helmholtz's decomposition relation for the displacement, we can obtain the sagittal plane displacement field of the j-th layer [64,45]. Then, the continuous displacement boundary conditions at the layer interface (i.e., $x_2 = 0$) result in the following generalized elastodynamic Snell's law [45,49,51]:

$$\begin{aligned} &\hat{\kappa}^R_{p,1}\sin\theta_{p,1} = \hat{\kappa}^R_{s,1}\sin\theta_{s,1} = \hat{\kappa}^R_{p,2}\sin\theta_{p,j} = \hat{\kappa}^R_{s,2}\sin\theta_{s,2}, \\ &\hat{\kappa}^I_{p,1}\sin\left(\theta_{p,1} + \zeta_{p,1}\right) = \hat{\kappa}^I_{s,1}\sin\left(\theta_{s,1} + \zeta_{s,1}\right) \\ &\quad = \hat{\kappa}^I_{p,2}\sin\left(\theta_{p,2} + \zeta_{p,2}\right) = \hat{\kappa}^I_{s,2}\sin\left(\theta_{s,2} + \zeta_{s,2}\right) \end{aligned} \tag{15}$$

where the first relation is obtained from the equality of real-valued components, whereas the second one is from that of imaginary-valued components.

Now, we study a special case where the first layer ($j=1$) is elastic, while the second layer ($j=2$) is viscoelastic (see Fig. 3(*a*)). Due to the nondissipative behavior of the elastic solid (i.e., $\boldsymbol{\kappa}^I_{p,1} = \boldsymbol{\kappa}^I_{s,1} = 0$ and see Eq. (10)), the wavevector relating to the first elastic layer should be real-valued, and subsequently its imaginary components in the displacement field should vanish as well. Consequently, the second equation in the generalized elastodynamic Snell's law (15) becomes [52]

$$\hat{\kappa}^I_{p,2} \sin\left(\theta_{p,2} + \zeta_{p,2}\right) = \hat{\kappa}^I_{s,2} \sin\left(\theta_{s,2} + \zeta_{s,2}\right) = 0 \tag{16}$$

which determines the attenuation angle in the second viscoelastic layer

$$\zeta_{p,2} = -\theta_{p,2}, \quad \zeta_{s,2} = -\theta_{s,2} \tag{17}$$

The above constraint (17) driven by using the elastodynamic Snell's law implies that wave attenuation in the viscoelastic layer occurs only in the direction perpendicular the layers (i.e., $\mathbf{n}^I_{p,2} \cdot \mathbf{e}_1 = \mathbf{n}^I_{s,2} \cdot \mathbf{e}_1 = 0$) regardless of wave propagation directions (see Fig. 3). In other words, while their κ_2-components remain complex, the κ_1-component of all the wavevectors becomes real

$$\boldsymbol{\kappa}^I_{r,j} \cdot \mathbf{e}_1 = \kappa^I_{r,j,1} = 0, \quad \text{for} \quad r = p, s \quad \text{and} \quad j = 1, 2 \tag{18}$$

where $\kappa^I_{r,j,1}$ denotes the κ_1-component of $\boldsymbol{\kappa}^I_{r,j}$. Furthermore, a similar conclusion can be obtained from the case where the second layer is elastic, while the first layer is viscoelastic, as shown in Fig. 3(*b*). In this case, an incident wave oblique to the viscoelastic layer attenuates within the viscoelastic layer in the direction dictated by the attenuation angle ζ. However, the reflected wave at the viscoelastic-elastic layer interface will attenuate only in the direction perpendicular to the layer following the elastodynamic Snell's law.

In summary, due to the nondissipative characteristics of the adjacent elastic layer, the wave attenuation behavior in viscoelastic-elastic interfaces is different from that in homogeneous viscoelastic solids or viscoelastic layered composites. Within each interspersed viscoelastic layer, the wave propagation direction may have a component parallel to the layer as shown in Fig. 3. However, the existence of interspersed elastic layer prevents the wave attenuation component parallel to the layer, and this argument is also discussed in Refs. [46], [47], and [52]. In particular, this characteristic is noteworthy to the study of wave analysis in alternating viscoelastic-elastic layered composites. Although incident waves within each individual viscoelastic layer attenuate in the direction dictated by the attenuation angle, reflected and refracted waves (i.e., resulting propagating waves) in the layered composites do not attenuate in the direction parallel to the layers due to the existence of elastic layers. This compelling wave characteristic of elastic-viscoelastic interfaces will be employed to investigate the analytical dispersion relation of alternating elastic-viscoelastic multilayered composites in Sec. 2.3.

2.3 Sagittal Plane Waves in Periodic Multilayered Composites Composed of Alternating Viscoelastic and Elastic Solids.

The analytical dispersion relation of elastic multilayered composites has been reported for sagittal plane waves at arbitrary directions [25,26,28]. Assuming harmonic wave motion, the solution of a viscoelastic problem is known to be similar to that of the elastic analog problem with elastic constants replaced by their viscoelastic counterpart [58]. However, there has been very little research on sagittal plane waves in viscoelastic multilayered composites because one cannot directly apply the analytical approach developed for elastic multilayered composites to the case of viscoelastic multilayered composites due to intricate wave attenuation characteristics at layer interfaces [45,49,51]. The challenge is briefly described in the following.

In the case of elastic multilayered composites, the dispersion relation of sagittal plane wave needs to be presented in a three-dimensional (3D) $\omega - \boldsymbol{\kappa}$ plot, i.e., ω over the $\kappa_1 - \kappa_2$ plane, where both κ_1 and κ_2 are real-valued. For instance, considering the symmetry of multilayered composites shown in Fig. 1, the valid range for the κ_1-axis is $\kappa_1 \in (0, \infty)$, while κ_2 should range over the first irreducible Brillouin zone (IBZ), i.e., $\kappa_2 \in (0, \pi/a_2)$, where a_2 is the unit-cell length [28,65]. Typically, the governing equation can be solved to find κ_2 for a given real-valued set of (κ_1, ω). Then, by sweeping $\kappa_1 \in [0, \infty)$ and $\omega \in [0, \infty)$, one can obtain the complete picture of the dispersion relations of elastic multilayered composites [21–26,28].

On the other hand, sagittal plane waves in viscoelastic multilayered composites are described by using a complex wavevector $\boldsymbol{\kappa} = [\kappa_1\ \kappa_2]^{\mathrm{T}}$, where both κ_1 and κ_2 are complex-valued. Accordingly, in the case of viscoelastic multilayered composites, the complete dispersion relation of sagittal plane waves needs to be presented in a plot of ω over $\boldsymbol{\kappa}$ $(= \boldsymbol{\kappa}^R + i\,\boldsymbol{\kappa}^I)$ domain, which cannot be represented in the conventional 3D space. Thus, the analytical approach sweeping a real-valued wavenumber over a domain cannot be applicable to the arbitrary viscoelastic multilayered composites, where the wavevector κ_1 is complex-valued. However, when the viscoelastic layer is attached to an elastic layer, Eq. (18) indicates that wave attenuation in a viscoelastic layer occurs only in the direction perpendicular to the layers, i.e., zero κ_1-component of $\boldsymbol{\kappa}^I$. Thus, this wave propagation characteristic (i.e., real-valued κ_1-component) enables us to directly apply the analytical approach employed in elastic multilayered composites to the dispersion relation of alternating viscoelastic-elastic multilayered composites. Based on our previous study on the elastic multilayered composites [28], we present a brief procedure in the remainder of this subsection.

As illustrated in Fig. 1(*a*), we consider a multilayered composite composed of alternating viscoelastic and elastic solids. The considered composite has M layers per unit cell, and it is infinitely periodic along the x_2-axis. The sagittal plane for this composite is given by the $x_1 - x_2$ plane, and the corresponding wavevector domain is represented by the $\kappa_1 - \kappa_2$ plane, where κ_1 is *real-valued* while κ_2 is *complex-valued*. The j-th layer of the composite has thickness d_j, so that the periodic unit-cell length a_2 of the composite is obtained by $a_2 = \sum_{j=1}^{M} d_j$. In addition, $x_{2,j,n}$ represents the local x_2-coordinate for the j-th layer. Note that a subscript j is employed to refer the characteristics of the j-th layer (e.g., $\hat{\lambda}_j$, $\hat{\mu}_j$, $c_{p,j}$, $c_{s,j}$, $\kappa_{p,j}$, $\kappa_{s,j}$).

The general solution of the potentials for the sagittal plane wave motion in the j-th layer is presented in Eq. (13). Applying this general solution to Helmholtz's decomposition, we obtain the displacement field of sagittal plane waves for the j-th layer in the n-th unit cell of the multilayered composite

$$\begin{aligned}
\bar{u}_{1,j,n}(x_1, x_{2,j,n}) &= \frac{\partial \bar{\Phi}_j}{\partial x_1} + \frac{\partial \bar{H}_{3,j}}{\partial x_{2,j,n}} \\
&= \left[-\frac{\kappa_1}{\alpha_{p,j}} P_{F,j,n} e^{-i\alpha_{p,j} x_{2,j,n}} + \frac{\kappa_1}{\alpha_{p,j}} P_{B,j,n} e^{i\alpha_{p,j} x_{2,j,n}} \right. \\
&\quad \left. + Q_{F,j,n} e^{-i\alpha_{s,j} x_{2,j,n}} + Q_{B,j,n} e^{i\alpha_{s,j} x_{2,j,n}} \right] e^{i\kappa_1 x_1}, \\
\bar{u}_{2,j,n}(x_1, x_{2,j,n}) &= \frac{\partial \bar{\Phi}_j}{\partial x_{2,j,n}} - \frac{\partial \bar{H}_{3,j}}{\partial x_1} \\
&= \left[P_{F,j,n} e^{-i\alpha_{p,j} x_{2,j,n}} + P_{B,j,n} e^{i\alpha_{p,j} x_{2,j,n}} + \frac{\kappa_1}{\alpha_{s,j}} Q_{F,j,n} e^{-i\alpha_{s,j} x_{2,j,n}} \right. \\
&\quad \left. - \frac{\kappa_1}{\alpha_{s,j}} Q_{B,j,n} e^{i\alpha_{s,j} x_{2,j,n}} \right] e^{i\kappa_1 x_1}
\end{aligned} \tag{19}$$

where $\alpha_{p,j} = \sqrt{\left[\kappa_{p,j}(\omega)\right]^2 - \kappa_1^2}$ and $\alpha_{s,j} = \sqrt{\left[\kappa_{s,j}(\omega)\right]^2 - \kappa_1^2}$ are the frequency-dependent complex coefficients relating to the

propagation and attenuation angles; and $P_{F,j,n} = -i\alpha_{p,j}\bar{\phi}_{F,j}$, $P_{B,j,n} = i\alpha_{p,j}\bar{\phi}_{B,j}$, $Q_{F,j,n} = -i\alpha_{s,j}\bar{h}_{F,j}$, and $P_{B,j,n} = i\alpha_{s,j}\bar{h}_{B,j}$ are the frequency-dependent complex amplitudes to be determined from boundary conditions. Moreover, the stress field can also be obtained for the j-th layer of n-th unit cell

$$\begin{aligned}
\bar{\sigma}_{21,j,n}(x_1, x_{2,j,n}) &= \hat{\mu}_j\left(2\frac{\partial^2\bar{\Phi}_j}{\partial x_1 \partial x_3} - \frac{\partial^2\bar{H}_{3,j}}{\partial x_1^2} + \frac{\partial^2\bar{H}_{3,j}}{\partial x_{2,j,n}^2}\right) \\
&= \hat{\mu}_j\left[2P_{F,j,n}\kappa_1 e^{-i\alpha_{p,j}x_{2,j,n}} + 2P_{B,j,n}\kappa_1 e^{i\alpha_{p,j}x_{2,j,n}} \quad + Q_{F,j,n}\frac{\left(\kappa_1^2 - \alpha_{s,j}^2\right)}{\alpha_{s,j}} e^{-i\alpha_{s,j}x_{2,j,n}} - Q_{B,j,n}\frac{\left(\kappa_1^2 - \alpha_{s,j}^2\right)}{\alpha_{s,j}} e^{i\alpha_{s,j}x_{2,j,n}}\right] e^{i\kappa_1 x_1}, \\
\bar{\sigma}_{22,j,n}(x_1, x_{2,j,n}) &= \left(\hat{\lambda}_j + 2\hat{\mu}_j\right)\left(\frac{\partial^2\bar{\Phi}_j}{\partial x_1^2} + \frac{\partial^2\bar{\Phi}_j}{\partial x_{2,j,n}^2}\right) - 2\hat{\mu}_j\left(\frac{\partial^2\bar{\Phi}_j}{\partial x_1^2} + \frac{\partial^2\bar{H}_{3,j}}{\partial x_1 \partial x_{2,j,n}}\right) \\
&= \left[-P_{F,j,n}\frac{\left(\hat{\lambda}_j + 2\hat{\mu}_j\right)\alpha_{p,j}^2 + \hat{\lambda}_j\kappa_1^2}{\alpha_{p,j}} e^{-i\alpha_{p,j}x_{2,j,n}} + P_{B,j,n}\frac{\left(\hat{\lambda}_j + 2\hat{\mu}_j\right)\alpha_{p,j}^2 + \hat{\lambda}_j\kappa_1^2}{\alpha_{p,j}} e^{i\alpha_{p,j}x_{2,j,n}} \quad -2Q_{F,j,n}\hat{\mu}_j\kappa_1 e^{-i\alpha_{s,j}x_{2,j,n}} - 2Q_{B,j,n}\hat{\mu}_j\kappa_1 e^{i\alpha_{s,j}x_{2,j,n}}\right] e^{i\kappa_1 x_1}
\end{aligned} \tag{20}$$

Here, for the j-th layer in the n-th unit-cell, we introduce a complex-valued amplitude vector $\mathbf{W}_{j,n}$

$$\mathbf{W}_{j,n} = \begin{bmatrix} P_{F,j,n} \\ P_{B,j,n} \\ Q_{F,j,n} \\ Q_{B,j,n} \end{bmatrix} \tag{21}$$

Then, the successive application of the continuous displacement and stress boundary conditions to all the layer interfaces in n-th unit-cell results in the following relation between the adjacent unit-cells [28]:

$$\mathbf{W}_{1,n+1} = \mathbf{T}\mathbf{W}_{1,n} \tag{22}$$

where

$$\mathbf{T} = \mathbf{T}(\omega, \kappa_1) = \mathbf{R}_1^{-1}\left(\prod_{j=2}^{M}\mathbf{R}_{M+2-j}\mathbf{D}_{M+2-j}\mathbf{R}_{M+2-j}^{-1}\right)\mathbf{R}_1\mathbf{D}_1 \tag{23}$$

$$\mathbf{R}_j = \begin{bmatrix} 1 & 1 & \frac{\kappa_1}{\alpha_{s,j}} & -\frac{\kappa_1}{\alpha_{s,j}} \\ -\frac{\left(\hat{\lambda}_j + 2\hat{\mu}_j\right)\alpha_{p,j}^2 + \hat{\lambda}_j\kappa_1^2}{\alpha_{p,j}} & \frac{\left(\hat{\lambda}_j + 2\hat{\mu}_j\right)\alpha_{p,j}^2 + \hat{\lambda}_j\kappa_1^2}{\alpha_{p,j}} & -2\hat{\mu}_j\kappa_1 & -2\hat{\mu}_j\kappa_1 \\ -\frac{\kappa_1}{\alpha_{p,j}} & \frac{\kappa_1}{\alpha_{p,j}} & 1 & 1 \\ 2\hat{\mu}_j\kappa_1 & 2\hat{\mu}_j\kappa_1 & \frac{\hat{\mu}_j\left(\kappa_1^2 - \alpha_{s,j}^2\right)}{\alpha_{s,j}} & -\frac{\hat{\mu}_j\left(\kappa_1^2 - \alpha_{s,j}^2\right)}{\alpha_{s,j}} \end{bmatrix} \tag{24}$$

$$\mathbf{D}_j = \begin{bmatrix} e^{-i\alpha_{p,j}d_j} & 0 & 0 & 0 \\ 0 & e^{i\alpha_{p,j}d_j} & 0 & 0 \\ 0 & 0 & e^{-i\alpha_{s,j}d_j} & 0 \\ 0 & 0 & 0 & e^{i\alpha_{s,j}d_j} \end{bmatrix} \tag{25}$$

where $\mathbf{T}$ is the transfer matrix determining the relation between the complex-valued amplitude vectors of adjacent unit-cells in the sagittal plane. Note that the obtained transfer matrix for the sagittal plane of alternating viscoelastic-elastic multilayered composites is analogous to its elastic counterpart derived in our previous study [28]. In addition, the Bloch periodic condition provides the second relation between adjacent unit-cells [66]

$$\mathbf{W}_{1,n+1} = e^{i\kappa_2 a_2}\mathbf{W}_{1,n} \tag{26}$$

Now, the substitution of the Bloch periodic condition (26)–(22) provides an eigenvalue problem

$$\mathbf{T}\mathbf{W}_{1,n} = e^{i\kappa_2 a_2}\mathbf{W}_{1,n} \tag{27}$$

where $e^{i\kappa_2 a_2}$ and $\mathbf{W}_{1,n}$ are the eigenvalue and the eigenvector of the transfer matrix $\mathbf{T}$, respectively. For a given set of a real-valued wavenumber $\kappa_1 \in [0, \infty)$ and a real-valued angular frequency $\omega \in [0, \infty)$, the eigenvalue problem can be solved to obtain a nontrivial complex-valued amplitude vector $\mathbf{W}_{1,n}$ and the corresponding complex-valued wavenumber κ_2. By setting $e^{i\kappa_2 a_2} = \eta$, Cayley–Hamilton theorem [67] provides the fourth-order characteristic polynomial of the transfer matrix $\mathbf{T}$

$$\eta^4 - g_3\eta^3 + g_2\eta^2 - g_1\eta + g_0 = 0 \tag{28}$$

where

$$\begin{aligned} g_3(\omega,\kappa_1) &= g_1(\omega,\kappa_1) = \mathrm{tr}(\mathbf{T}),\\ g_2(\omega,\kappa_1) &= \frac{1}{2}\left[(\mathrm{tr}(\mathbf{T}))^2 - \mathrm{tr}(\mathbf{T}^2)\right],\\ g_0(\omega,\kappa_1) &= 1 \end{aligned} \tag{29}$$

Here, the symmetry of the solutions is adopted to simplify the polynomial coefficients $g_3 = g_1$ and $g_0 = 1$ [28]. Consequently, for a given real-valued set of (κ_1, ω), a complex-valued wavenumber κ_2 can be determined by solving the characteristic polynomial (28) [28] and it is eventually determined from the following nonlinear equation:

$$\cos(\kappa_2 a_2) = \frac{1}{4}\left[g_3(\omega,\kappa_1) \pm \sqrt{[g_3(\omega,\kappa_1)]^2 - 4g_2(\omega,\kappa_1) + 8}\right] \tag{30}$$

It is again worth mentioning that the obtained dispersion relation (30) of sagittal plane waves for alternating viscoelastic-elastic multilayered composites is similar to its elastic counterpart derived in our previous study [28], except that material properties $\hat{\lambda}(\omega)$ and $\hat{\mu}(\omega)$ are frequency-dependent and complex-valued in this study. Interested readers may refer to our previous study [28] on the dispersion relation of infinitely periodic multilayered elastic composites.

3 Results

In this section, we consider a specific periodic bilayered composite composed of alternating a metal and a viscoelastic polymer and investigate the dispersion relation of sagittal plane waves at four different angles: $\theta = 0\,\mathrm{deg}$, $15\,\mathrm{deg}$, $30\,\mathrm{deg}$, and $60\,\mathrm{deg}$. Using Eq. (30), we obtain the analytical dispersion relation of the considered layered composite. In order to illustrate the distinct effects of viscoelastic properties, we also consider an elastic counterpart of the alternating polymer-metal composite, taking only the static, elastic properties of the polymer and neglecting its damping properties. In addition to the complex-valued dispersion relation, the transmission coefficient and the group slowness are calculated.

3.1 Geometry and Materials of the Considered Composite.

To study the dispersion relation of sagittal plane waves, we consider a specific bilayered composite composed of alternating aluminum (aluminum 6061-T6) and polyurethane elastomer (Hapflex-560 from Hapco Inc., Hanover, MA). The subscripts 1 and 2 denote the aluminum layer and the polyurethane layer, respectively. The unit-cell of the composite comprises an aluminum layer of $d_1 = 10\,\mathrm{mm}$ and a polyurethane layer of $d_2 = 10\,\mathrm{mm}$, so that the unit-cell length along the x_2-axis is $a_2 = d_1 + d_2 = 20\,\mathrm{mm}$.

For the material properties of aluminum, we use the mass density of $\rho_1 = 2700\,\mathrm{kg/m^3}$ and the frequency-independent elastic moduli of $\lambda_1 = 51.1\,\mathrm{GPa}$ and $\mu_1 = 26.3\,\mathrm{GPa}$. On the other hand, the complex-valued viscoelastic moduli of the considered polyurethane are experimentally determined by performing dynamic mechanical analysis (DMA) using RSA-G2 Solids Analyzer from TA Instruments. Two different samples were tested, and the deviation was very small, showing only around 1% for both storage and loss modulus of polyurethane elastomer. From the experiments, we obtain the complex-valued tensile modulus $\hat{E}_2(\omega) = \hat{E}_2'(\omega) + i\hat{E}_2''(\omega)$ and shear modulus $\hat{\mu}_2(\omega) = \hat{\mu}_2'(\omega) + i\hat{\mu}_2''(\omega)$, where $\square'$ and $\square''$ denote the storage modulus and the loss modulus, respectively. Then, $\hat{\lambda}_2(\omega)$ is determined through the relation $\hat{\lambda}_2 = \left(\hat{\mu}_2(\hat{E}_2 - 2\hat{\mu}_2)\right)/(3\hat{\mu}_2 - \hat{E}_2)$. The experimentally obtained complex moduli (i.e., $\hat{\lambda}_2(\omega)$ and $\hat{\mu}_2(\omega)$) of polyurethane are presented in Fig. 4, where the linear frequency denoted by $f = \omega/(2\pi)$ is employed instead of the angular frequency ω. The mass density of the considered polyurethane is $\rho_2 = 1060\,\mathrm{kg/m^3}$.

In order to highlight the effects of viscoelastic properties in the dispersion analysis of sagittal plane waves, we explore two sets of material models for the considered composite: one set with elastic aluminum and viscoelastic polyurethane models and the other with elastic aluminum and *pseudo*-elastic polyurethane models. Here, for pseudo-elastic polyurethane model, we extract the frequency-independent elastic moduli (i.e., $\hat{\lambda}_2^{pe} = 41.5\,\mathrm{MPa}$ and $\hat{\mu}_2^{pe} = 6.76\,\mathrm{MPa}$; see the dotted lines in Fig. 4) from its storage

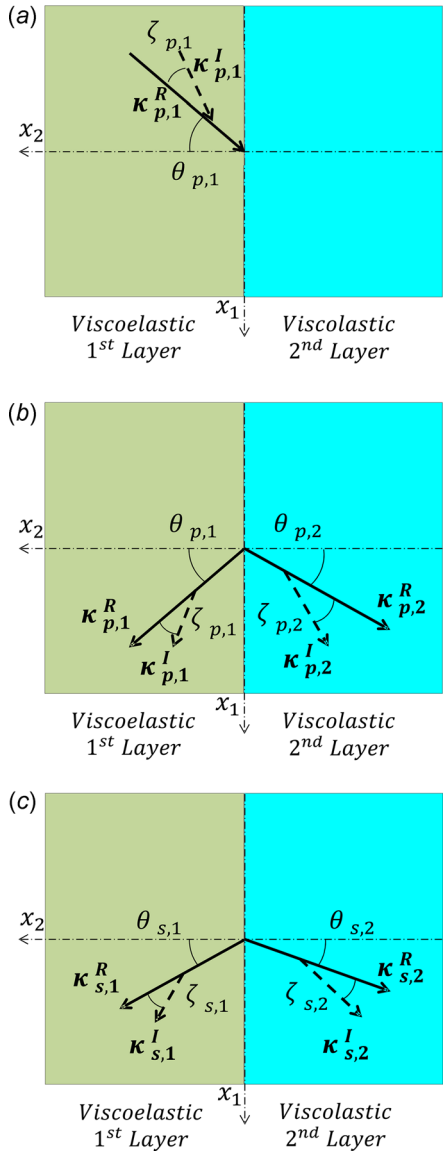

Fig. 2 (*a*) P-wave with a wavevector $\kappa_{p,1}$ (i.e., $\kappa_{p,1} = \kappa_{p,1}^R + i\kappa_{p,1}^I$) incidents at the interface between viscoelastic layers 1 and 2 with a propagation angle $\theta_{p,1}$ and an attenuation angle $\zeta_{p,1}$. (*b*) Reflected and transmitted P-waves in layers 1 and 2, respectively. The propagation and attenuation wavevectors are represented by $\kappa_{p,j}^R$ and $\kappa_{p,j}^I$ (for $j = 1, 2$), respectively. (*c*) Reflected and transmitted SV-waves in layers 1 and 2, respectively. The propagation and attenuation wavevectors are represented by $\kappa_{s,j}^R$ and $\kappa_{s,j}^I$ (for $j = 1, 2$), respectively. Note that the angles of propagation and attenuation waves are denoted by $\theta_{r,j}$ and $\zeta_{r,j}$ (for $j = 1, 2$ and $r = p, s$), respectively.

moduli at the zero frequency ($f = 0$), which can be viewed as a long-term static behavior.

3.2 Complex-Valued Dispersion Relations. For the considered periodic bilayered composite composed of alternating polyurethane and aluminum, the analytical expression of the dispersion relation (30) can provide the complete dispersion relation of the sagittal plane in the complex wavevector domain. Here, due to the existence of elastic layers, plane waves attenuate only in the direction perpendicular to the layers (i.e., $\boldsymbol{\kappa}^I \cdot \mathbf{e}_1 = 0$ and see Fig. 3), so the propagation and the attenuation characteristics of sagittal plane waves can be formally presented in the two 3D plots of ω over the $\kappa_1^R - \kappa_2^R$ plane and ω over the $\kappa_1^R - \kappa_2^I$ plane. In this study, the effects of viscoelasticity on sagittal plane waves are investigated by considering harmonic plane waves at four different incident angles, $\theta = 0$ deg, 15 deg, 30 deg, and 60 deg, where $\theta = \cos^{-1}\left(\boldsymbol{\kappa}^R/||\boldsymbol{\kappa}^R|| \cdot \mathbf{e}_2\right)$ (see Fig. 1). By considering the symmetricity of wave motion, we present the dispersion relation of sagittal plane waves at the propagation angle of θ in two 2D plots: one with $\kappa_\theta^R - f$ and the other with $\kappa_2^I - f$, where

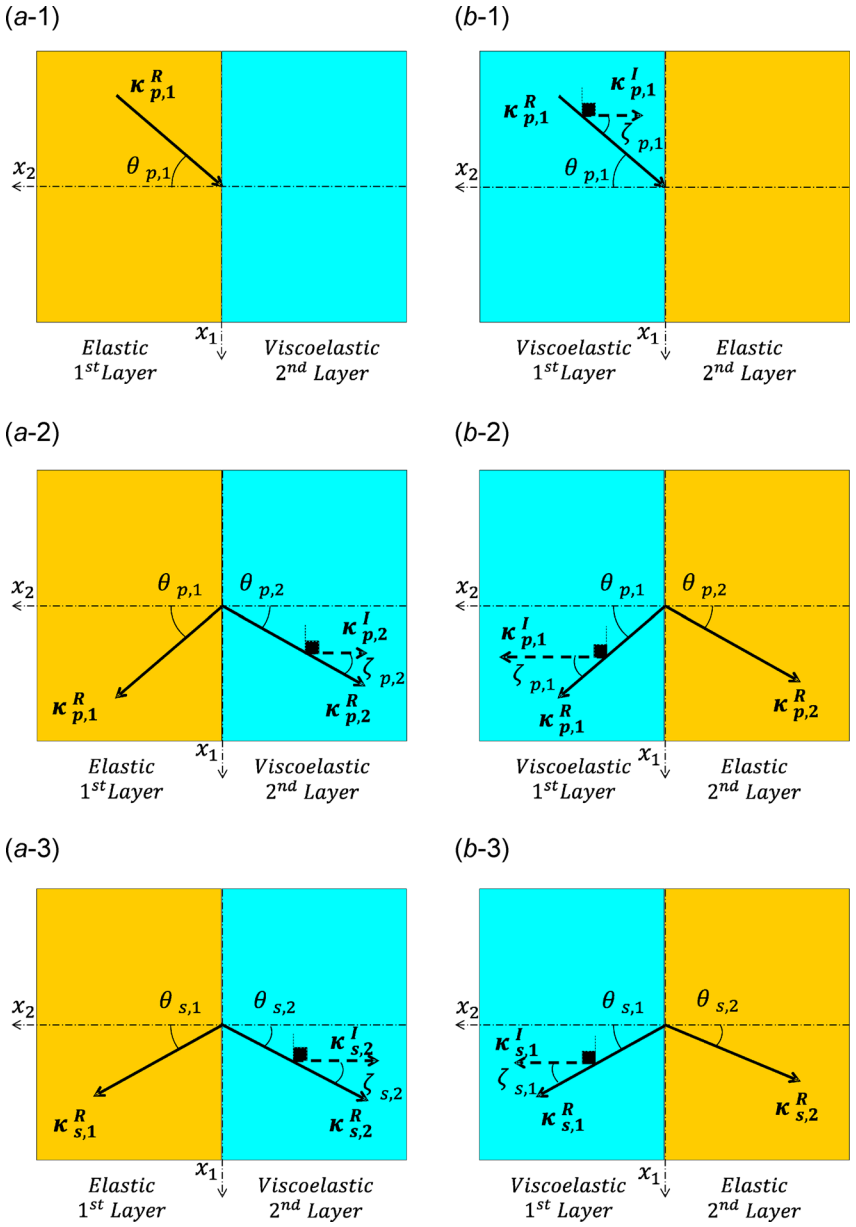

Fig. 3 (*a*-1) Incident P-wave having a wavevector $\kappa_{p,1}^R$ at an angle $\theta_{p,1}$ from the elastic medium at the interface between elastic and viscoelastic layers 1 and 2. Reflected and transmitted (*a*-2) P-waves and (*a*-3) SV-waves having characterized by the propagation wavevectors $\kappa_{r,j}^R$ (for $j = 1, 2$ and $r = p, s$) for both layers and the attenuation wavevectors $\kappa_{r,2}^I$ for the viscoelastic layer. (*b*-1) Incident P-wave having a wavevector $\kappa_{p,1}^R$ at an angle $\theta_{p,1}$ from the viscoelastic medium at the interface between elastic and viscoelastic layers 1 and 2. Reflected and transmitted (*b*-2) P-waves and (*b*-3) SV-waves having characterized by the propagation wavevectors $\kappa_{r,j}^R$ (for $j = 1, 2$ and $r = p, s$) for both layers and the attenuation wavevectors $\kappa_{r,2}^I$ for the viscoelastic layer. Note that the propagation angles in the layers are denoted by $\theta_{r,j}$ and the attenuation angles in the viscoelastic layer are shown by $\zeta_{r,2}$.

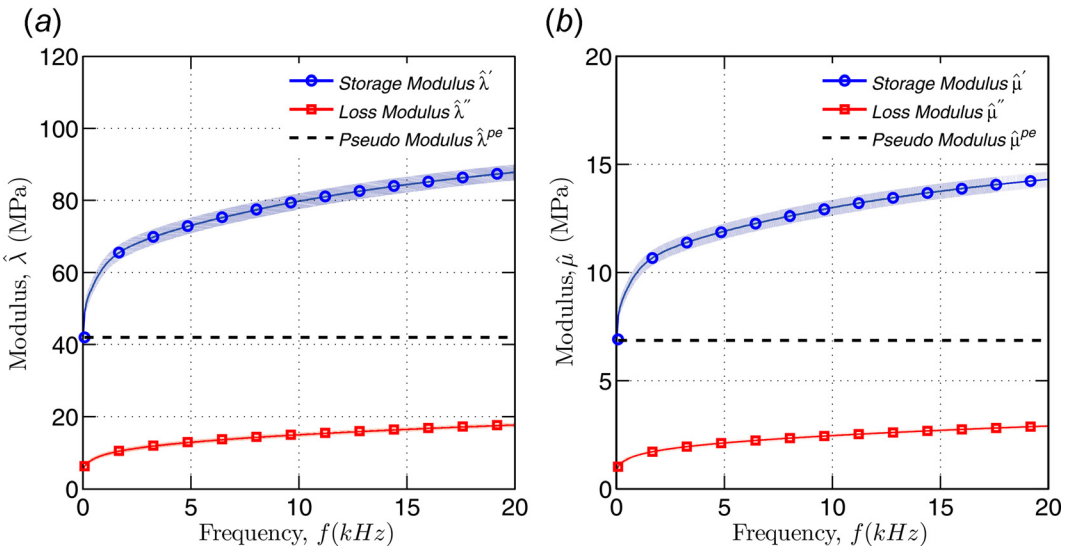

Fig. 4 Viscoelastic properties of polyurethane elastomer obtained by DMA. (*a*) Frequency-dependent modulus $\hat{\lambda}(\omega)$. (*b*) Frequency-dependent modulus $\hat{\lambda}(\omega)$. The storage and the loss moduli are represented by circle- and square-marked solid lines, respectively. Note that the shaded areas denote one standard deviation from two DMA tests. The constant modulus of pseudo-elastic approximation is shown by dotted lines.

$\kappa_\theta^R = \kappa_2^R/\cos\theta$. Note that κ_θ^R denotes the wavenumber in the direction of the wave propagation angle θ, and the representation scheme is illustrated in Fig. 5. In other words, for a given real-valued set of (κ_1, ω), a complex-valued wavenumber κ_2 $(= \kappa_2^R + i\,\kappa_2^I)$ is calculated from Eq. (30). Then, the real component κ_θ^R is obtained from identifying the intersections of the θ-plane and the collection of the calculated κ_2^R. Accordingly, the associated imaginary component κ_2^I is found and is projected on the $\kappa_2^I - f$ plane. For a given frequency, we observe that more than two wave modes can exist at arbitrary oblique angles (see Figs. 6 and 7).

Figure 6 presents the dispersion relations of sagittal plane waves in the alternating polyurethane-aluminum bilayered composite, where polyurethane is modeled as a pseudo-elastic material model using elastic properties extracted from a long-term static behavior. Similarly, Fig. 7 shows the corresponding dispersion relations of the considered bilayered composite, where polyurethane is modeled as a viscoelastic material model using the measured complex moduli shown in Fig. 4. While the left columns of Figs. 6 and 7 show the wave attenuation characteristics represented in the $\kappa_2^I - f$ space, the right columns present the dispersion relation represented in the $\kappa_\theta^R - f$ space. Due to the application of the Bloch periodic boundary condition (26), the real part of wavenumber κ_θ^R (i.e., propagation characteristics) is confined within the IBZ (i.e., $\kappa_\theta^R \in [0, \pi/(a_2\cos\theta)]$) as shown in the right columns of Figs. 6 and 7. On the other hand, the left columns show that the imaginary part of wavenumber κ_2^I is unbounded (i.e., $\kappa_2^I \in [0, \infty)$) since wave attenuation is not restrained by the periodicity of the composite.

3.3 Group Slowness and Transmission Coefficient. In order to qualitatively investigate the wave transmission characteristics in the considered composite, we further calculate the group slowness and the transmission coefficient from the obtained dispersion relation. The group slowness S_g is defined as the inverse of group velocity [68], and it measures the rate of change in wavenumber with respect to angular frequency

$$S_g = \frac{d\kappa_\theta^R}{d\omega} \tag{31}$$

The group slowness has been adopted to investigate wave directionality in iso-frequency surfaces [69,70], locally resonant characteristics [71,72], and sound absorption [73,74]. Since its definition is closely related to the density of states, the group slowness also describes the number of wave modes per unit frequency range. In other words, high group slowness values at a specific frequency imply an abundance of wave modes in the considered media. In this study, the group slowness is calculated from the real part of the wavenumber κ_2 (i.e., recall $\kappa_\theta^R = \kappa_2^R/\cos\theta$), and it is presented in the right columns of Figs. 8 and 9 for the pseudo-elastic material model and the viscoelastic material model, respectively.

In addition to the group slowness which is governed by the phase of waves, we also compute the transmission coefficient from the imaginary part of the wavenumber κ_2. The transmission coefficient is commonly used to investigate the attenuation characteristics of periodic layered composites [5,20,75–80]. Recall that the Bloch periodic condition can also be established between n-th and $(n+N)$-th unit-cell amplitude vectors

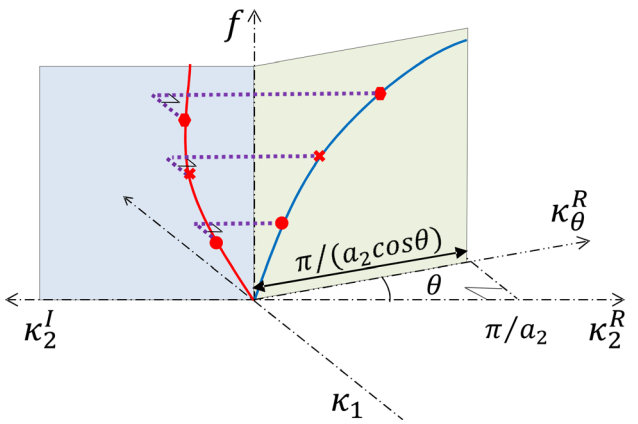

Fig. 5 A schematic view of representing the complex-valued dispersion relation ($\kappa = [\kappa_1\ \kappa_2^R]^T + i\,[0\ \kappa_2^I]^T$ and f) in the two-dimensional plots (i.e., $\kappa_\theta^R - f$ and $\kappa_2^I - f$). The phase dispersion relation is shown by a solid line in the wave propagation plane inclined at an angle θ on the $\kappa_1 - \kappa_2^R$ plane. The inclined length of the phase dispersion plane is $\pi/a_2\cos\theta$, 0 which is the projection length of π/a_2 on the κ_2^R-axis. As a demonstration, three exemplary points of $\kappa_\theta^R - f$ are projected on the $\kappa_2^I - f$ plane, which represents the corresponding attenuation relation.

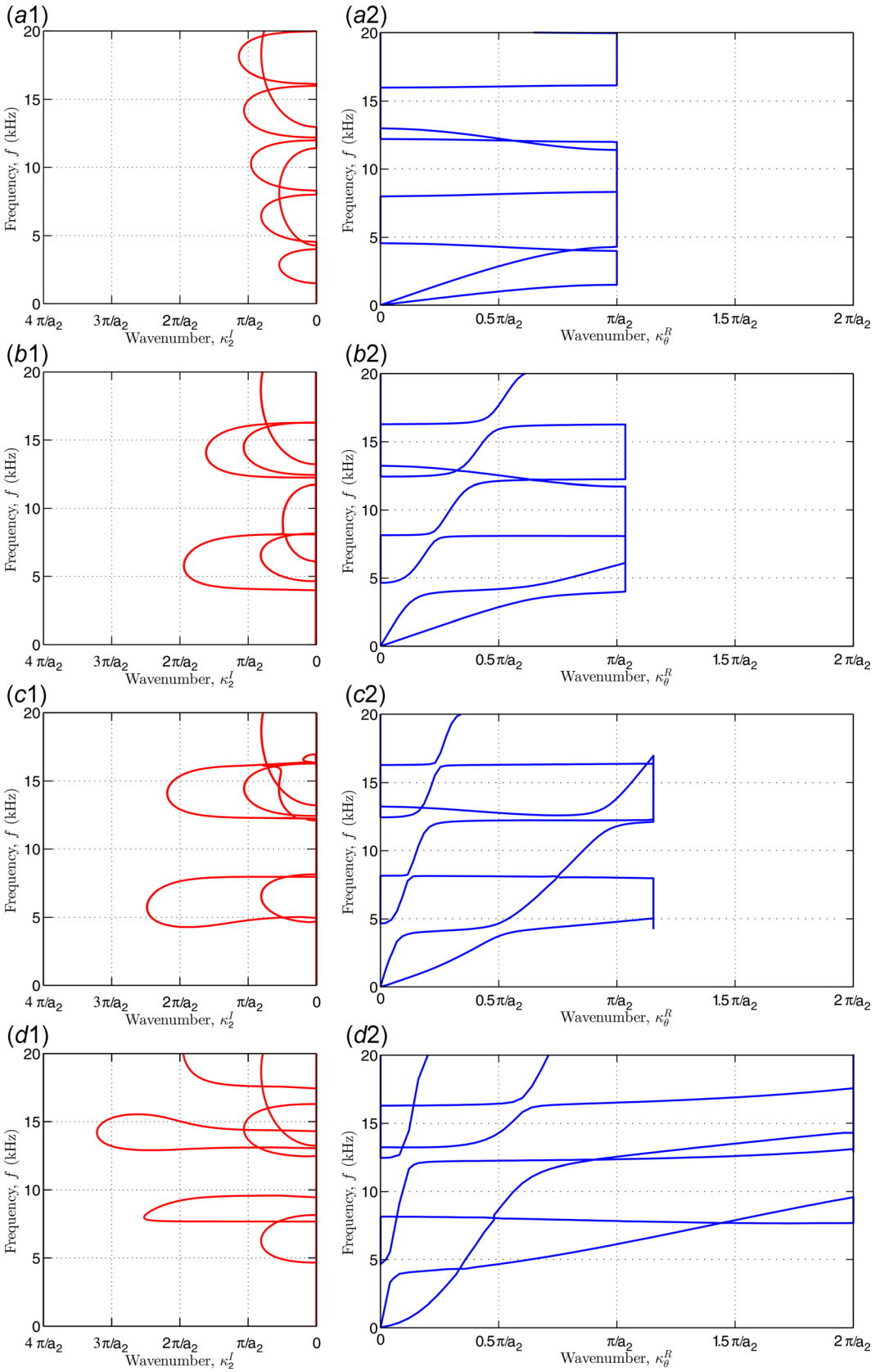

Fig. 6 Complete dispersion analysis results of the pseudo-elastic composite showing attenuation relations $\kappa_2^I - f$ for wave motions at (*a*-1) $\theta = 0$ deg, (*b*-1) $\theta = 15$ deg, (*c*-1) $\theta = 30$ deg, and (*d*-1) $\theta = 60$ deg. The phase dispersion relations $\kappa_\theta^R - f$ are illustrated for wave motions at (*a*-2) $\theta = 0$ deg, (*b*-2) $\theta = 15$ deg, (*c*-2) $\theta = 30$ deg, and (*d*-2) $\theta = 60$ deg. Note that the range of the wavevector $\kappa_\theta^R \in [0, \pi/(a_2 \cos\theta)]$ within the IBZ varies with the propagation angle.

$$\mathbf{W}_{1,n+N} = e^{i\kappa_2 Na_2}\mathbf{W}_{1,n} \tag{32}$$

where Na_2 denotes the distance between the two considered unit-cells. In this study, we define the transmission coefficient by taking the displacement amplitude ratio between an incident wave and the corresponding transmitted wave. By substituting $\kappa_2 = \kappa_2^R + i\,\kappa_2^I$, the transmission coefficient C_t is defined by

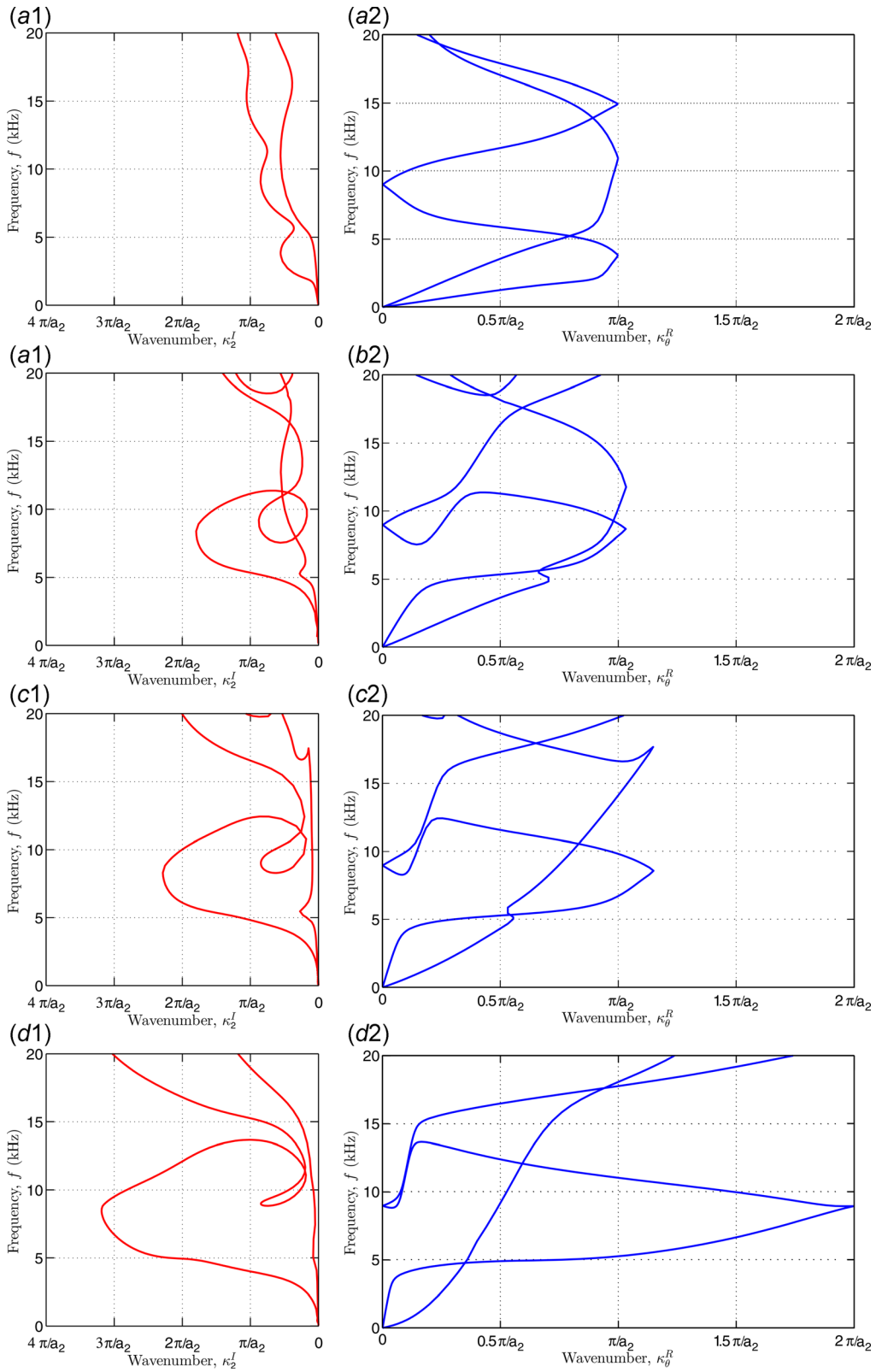

Fig. 7 Complete dispersion analysis results of the viscoelastic-elastic composite showing attenuation relations $\kappa_2^I - f$ for wave motions at (*a*-1) $\theta = 0$ deg, (*b*-1) $\theta = 15$ deg, (*c*-1) $\theta = 30$ deg, and (*d*-1) $\theta = 60$ deg. The phase dispersion relations $\kappa_\theta^R - f$ are illustrated for wave motions at (*a*-2) $\theta = 0$ deg, (*b*-2) $\theta = 15$ deg, (*c*-2) $\theta = 30$ deg, and (*d*-2) $\theta = 60$ deg. Note that the range of the wavevector $\kappa_\theta^R \in [0, \pi/(a_2 \cos\theta)]$ within the IBZ varies with propagation angles.

$$C_t = \frac{||\mathbf{W}_{1,n+N}||}{||\mathbf{W}_{1,n}||} = e^{-\kappa_2^I N a_2} \tag{33}$$

where the Euclidean norm $||\square||$ is adopted for the magnitude of the complex-valued amplitude vectors. Note that the transmission coefficient becomes unity (i.e., $C_t = 1$) as κ_2^I decreases to zero (i.e., $\kappa_2^I = 0$). On the other hand, the transmission coefficient converges to zero (i.e., $C_t = 0$) as N increases for $\kappa_2^I > 0$. The magnitude of the transmission coefficient of viscoelastic-elastic layered composites is significantly affected by N. In this study, the transmission coefficient is calculated by selecting $N = 3$ to highlight the difference of the transmission coefficient profiles. The left columns of Figs. 8 and 9 show the transmission coefficients of the pseudo-elastic material model and the viscoelastic material model, respectively. When it comes to the interpretation of the

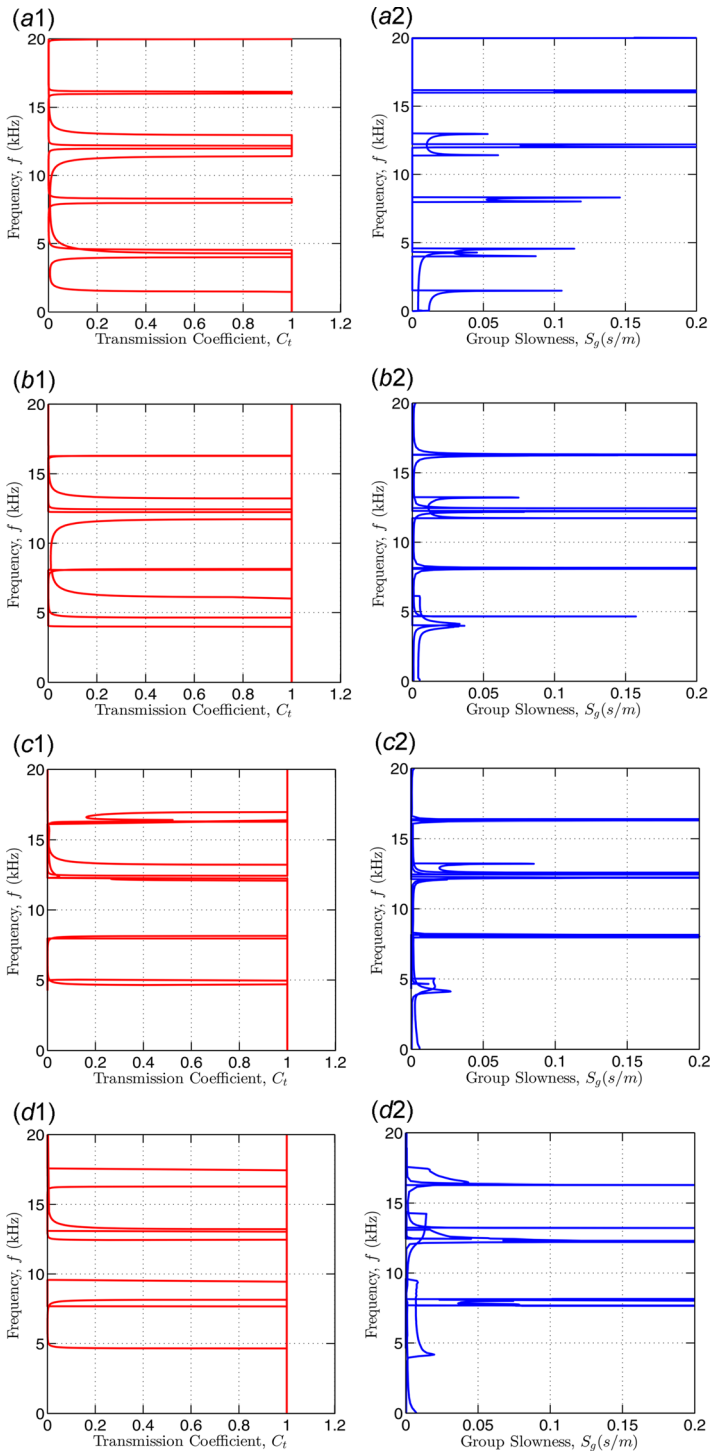

Fig. 8 Transmission coefficient C_t of the pseudo-elastic composite calculated from Eq. (33) for wave motion at (*a*-1) $\theta = 0$ deg, (*b*-1) $\theta = 15$ deg, (*c*-1) $\theta = 30$ deg, and (*d*-1) $\theta = 60$ deg. Group slowness S_g obtained using Eq. (31) for wave motion at (*a*-2) $\theta = 0$ deg, (*b*-2) $\theta = 15$ deg, (*c*-2) $\theta = 30$ deg, and (*d*-2) $\theta = 60$ deg.

attenuation characteristics of waves, a transmission coefficient plot is more practical than the attenuation plot of $\kappa_2^I - f$ because an experimentally measured transfer function can be directly comparable to the corresponding transmission coefficient plot.

4 Discussion

This section describes the outcome of various wave characteristic measures obtained from the analytical dispersion relation (30) regarding wave motion in the alternating viscoelastic-elastic infinitely periodic multilayered composites. In addition, we demonstrate that wave dispersion relation in viscoelastic-elastic layered composites is distinctly different from the corresponding elastic counterpart, and it highlights the importance of the viscoelastic modeling of polymeric materials in wave dispersion analysis.

4.1 Wave Characteristic Measures Obtained From Analytical Dispersion Relation. At oblique incident waves, Figs. 6 and 7 show the multimodal behavior (i.e., more than two modes)

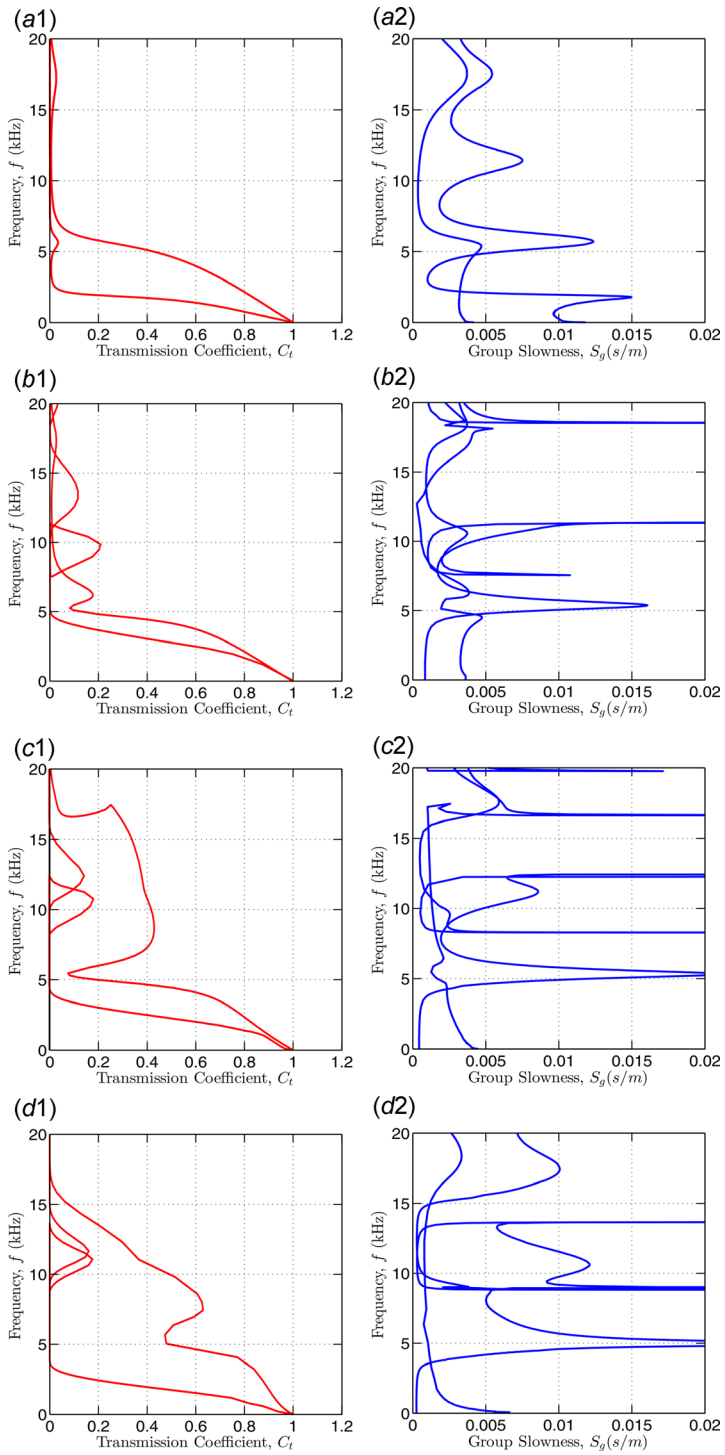

Fig. 9 Transmission coefficient C_t of periodic the viscoelastic-elastic composite calculated from Eq. (33) for wave motion at (*a*-1) $\theta = 0$ deg, (*b*-1) $\theta = 15$ deg, (*c*-1) $\theta = 30$ deg, and (*d*-1) $\theta = 60$ deg. Group slowness S_g obtained using Eq. (31) for wave motion at (*a*-2) $\theta = 0$ deg, (*b*-2) $\theta = 15$ deg, (*c*-2) $\theta = 30$ deg, and (*d*-2) $\theta = 60$ deg.

in $\kappa_\theta^R - f$ plots and spiral intersections in $\kappa_2^I - f$ plots. As we describe in Sec. 3.2, this phenomenon is indebted to the two-dimensional representation (i.e., $\kappa_\theta^R - f$ and $\kappa_2^I - f$) of the complex-valued dispersion relation (i.e., relation between $\boldsymbol{\kappa} = \left[\kappa_1\ \kappa_2^R\right]^{\mathrm{T}} + i\left[0\ \kappa_2^I\right]^{\mathrm{T}}$ and f) of the considered layered composite. As we illustrate in Fig. 5, the results shown in Figs. 6 and 7 can be viewed as the projection of the complex-valued dispersion relation onto the $\kappa_\theta^R - f$ and $\kappa_2^I - f$ planes for a given frequency value.

Wave propagation perpendicular to the layers is characterized by $\theta = 0$ (consequently, $\kappa_1 = 0$; see Fig. 5), and it contains only two uncoupled wave modes at any given frequency as shown in Figs. 6(*a*-1) and 7(*a*-1). For wave motion at oblique angles with $\theta > 0$, the wavenumber κ_1 varies within the Brillouin zone (i.e., $0 \le \kappa_1 \le (\pi/a_2)\tan\theta$), and Eq. (30) provides a pair of eigenvalues possessing coupled wave modes (see Ref. [28]). Note that the dispersion relations in Figs. 6 and 7 are obtained by intersecting the oblique $\kappa_\theta^R - f$ plane with the continuous evolution of the eigenvalue pair on the $\kappa_1 - f$ plane. Thus, the identified dispersion relation may result in more than two coupled modes on the projected $\kappa_\theta^R - f$ plane at a given frequency and may engender spiral intersections on the $\kappa_2^I - f$ plane (see Figs. 7(*b*)–7(*d*)). It is worth noting that the multimodal behavior on the $\kappa_\theta^R - f$ plane is accompanied by spiral intersections on the $\kappa_2^I - f$ plane. A representative example can be found near $f \approx 9$ kHz. Tamura and Wolfe [19] have also reported a similar phenomenon for wave motion at oblique angles in infinitely periodic elastic layered composites.

From the identified complex-valued dispersion relation from Eq. (30) (i.e., results in Figs. 6 and 7), we also analytically calculate the group slowness S_g and transmission coefficient C_t (see Figs. 8 and 9), which are frequently adopted to evaluate qualitatively the wave characteristics of phononic crystals. The physical meaning of the group slowness (see Eq. (31)) resembles that of the density of states, which measures the number of states (or wave modes) at each frequency. In other words, high group slowness values at a specific frequency imply an abundance of wave modes in the considered media. The high peaks in the group slowness plots (Figs. 8 and 9) correspond to nearly horizontal dispersion relation (i.e., $\kappa_\theta^R - f$ plot) in Figs. 6 and 7. On the other hand, the zero group slowness value indicates absolutely no wave propagation through the medium, and it clearly identifies the complete phononic band-gaps for the pseudo-elastic composite at the incident angle $\theta = 0$ deg (see Figs. 6(*a*-2) and 8(a-2)). For the viscoelastic-elastic layered composite, however, the group slowness investigation shows that there is no complete phononic band-gaps regardless of the incident angle due to the simultaneous wave propagation and attenuation in the medium (see Fig. 8, right column). Note that the behavior of the group slowness is highly localized along the frequency because it is defined by the derivatives of wavenumber with respect to frequency.

While the group slowness S_g focuses on wave modes in medium, the transmission coefficient C_t defined in Eq. (33) is relating to amplitude attenuation. A high transmission coefficient indicates low wave attenuation. In the pseudo-elastic layered composite, the maximum transmission coefficient value is predominantly one at oblique incident angles, indicating high wave transmission (see Fig. 8, left column). However, the transmission coefficient plots for the viscoelastic-elastic layered composite show a large wave attenuation only near a low frequency range (i.e., below 10 kHz). Furthermore, the spiral intersections observed in the $\kappa_2^I - f$ plot do not necessarily induce an abnormal wave attenuation behavior because the definition of the transmission coefficient is dependent on only the value of κ_2^I.

4.2 Pseudo-Elastic Layered Composite Versus Viscoelastic-Elastic Layered Composite. In the dispersion relation of pseudo-elastic layered composites, the wavenumber κ_2 can be among pure real number, pure imaginary number, or complex conjugate pair, which represent propagating band, attenuating band, and anticrossing band induced from the mixed mode interaction, respectively [19,29–32,81]. For waves perpendicular to the layers (i.e., $\theta = 0$ deg), the dispersion relation in Figs. 6(*a*-1) and 6(*a*-2) depicts several complete stop bands (e.g., around 5 kHz, 7 kHz, 12 kHz, 15 kHz), which are characterized by non-zero κ_2^I with an infinite group velocity $df/d\kappa_\theta^R$. Furthermore, we also confirm the existence of those stop bands from the transmission coefficient and the group slowness in Figs. 8(*a*-1) and 8(*a*-2). Note that vertical lines on the right edge of the dispersion relations $\kappa_\theta^R - f$ in the right columns of Fig. 6 represent a stop band for the considered wave mode, indicating $df/d\kappa_\theta^R = \infty$. However, all those complete stop bands disappear at oblique angles. In Figs. 8(*b*)–8(*d*) from the pseudo-elastic material model, we observe vertical lines in the transmission coefficient (i.e., $C_t = 1$), representing propagating wave modes with $\kappa_2^I = 0$. In other words, the transmission coefficient of unity in Figs. 8(*b*)–8(*d*) shows that there exists at least one propagating wave mode within the considered frequency ranges (i.e., up to 20 kHz).

On the other hand, Fig. 7 shows the dispersion relation of sagittal plane waves in the alternating polyurethane-aluminum bilayered composite, where polyurethane is modeled as a viscoelastic material using the measured complex moduli shown in Fig. 4. The wavenumber κ_2 in the dispersion relation of viscoelastic-elastic composite is always complex-valued due to the presence of inherent material damping of viscoelastic layers, implying that there are neither complete stop bands nor propagation bands without any attenuation. In other words, the dispersion relations of Fig. 7 illustrate that all the modes of sagittal plane waves in viscoelastic-elastic layered composites are simultaneously propagating and attenuating. No complete band-gap is observed even for wave propagation perpendicular to the layers [38,82], but Figs. 7 and 9 indicate that there exist some low wave transmission regions. For instance, Fig. 9(*a*-1) shows that frequency contents above 7 kHz at $\theta = 0$ deg substantially attenuate within a distance of three unit-cells (i.e., $N = 3$). This wave motion in viscoelastic-elastic layered composites is distinctly different from that in the elastic counterpart composites, whose analysis results are shown in Fig. 8(*a*-1). Similar trends can also be observed in the cases of different incident angles shown in the left column of Fig. 9. However, we find that wave motions at oblique angles can travel with a wide range of frequency contents, compared to the case of the incident angle of $\theta = 0$ deg. Note that the largest envelope of a transmission coefficient plot is determined by the smallest κ_2^I envelope due to the definition of the transmission coefficient in Eq. (33). Thus, the left column of Fig. 9 implies that the use of viscoelastic layers can prevent high frequency wave motions (e.g., >15 kHz), but there is not much attenuation in low frequency wave motions (e.g., <7 kHz) regardless of wave propagation directions. Consequently, Fig. 9 clearly shows that the viscoelastic material model reveals the distinctive wave attenuation, which cannot be captured by the pseudo-elastic material model (see Fig. 8). In addition, there is another noteworthy feature in the overall distribution of phase dispersion relation $\kappa_\theta^R - f$ of a viscoelastic-elastic layered composite, compared to that of the elastic counterpart. The right column of Fig. 7 shows that wave modes in viscoelastic-elastic layered composite are placed in the higher frequency ranges than those in the pseudo-elastic model, and this is due to the employment of the frequency-dependent moduli. Note that Fig. 4 exhibits that the frequency-dependent viscoelastic storage moduli of polyurethane is getting stiffer as frequency increases, whereas the pseudo-elastic material model has the frequency-independent elastic moduli.

5 Conclusion

In designing phononic crystals whose band-gaps are located in low-frequency ranges, researchers commonly adopt low stiffness polymeric materials as a key constituent to obtain the high impedance mismatch between metals and polymers. However, the majority of analytical and numerical studies on metal-polymer

dispersion relation consider only the elastic behavior of polymeric materials, ignoring their inherent viscoelastic properties. In this study, we analytically investigate dispersion relation for oblique wave motion in the sagittal plane of infinitely periodic multilayered composite composed of alternating viscoelastic and elastic solids, where the attenuation of harmonic plane waves is found to occur only in the direction perpendicular to the layers. By using this wave propagation characteristic, we directly apply the semi-analytical approach employed in elastic multilayered composites to find the dispersion relation of sagittal plane waves in alternating viscoelastic-elastic multilayered composites.

Furthermore, this study shows that the presented analytical dispersion relation can provide various wave characteristic measures in the alternating viscoelastic-elastic infinitely periodic multilayered composites. We consider a specific bilayered composite composed of alternating aluminum and polyurethane elastomer, whose complex-valued viscoelastic moduli are experimentally determined by performing DMA. In order to illustrate the distinct effects of its viscoelastic properties, the wave motion of the alternating viscoelastic-elastic layered composite is compared with that of its elastic counterpart, where the frequency-independent elastic moduli of polyurethane elastomer are extracted from its storage moduli at the zero frequency. The analysis shows that the alternating viscoelastic-elastic layered composite does not possess a phononic band-gap, regardless of incident angles. In addition, wave motions at oblique angles (other than $\theta = 0\,\text{deg}$) are found to travel with a wide range of frequency contents, compared to wave motion perpendicular to the layers. Importantly, the presented analysis demonstrates that the wave dispersion relation in viscoelastic-elastic layered composites is distinctly different from the corresponding elastic counterpart, and highlights the importance of the viscoelastic modeling of polymeric materials in wave dispersion analysis. Currently, we are working on experiments to validate the analytical results presented in this study.

Acknowledgment

The authors thank Qatar University Center for Advanced Materials and Professor Mitchell Anthamatten at the University of Rochester for facilitating the DMA tests of the considered polyurethane. Thanks are also due to the support of the Center for Computational Research at the University at Buffalo (UB).

Funding Data

- Qatar National Research Fund (Grant No. NPRP8-1568-2-666).

References

[1] Cao, W. W., and Qi, W. K., 1995, "Plane Wave Propagation in Finite Composites," J. Appl. Phys., **78**(7), pp. 4627–4632.
[2] Zhang, V. Y., Lefebvre, J. E., and Gryba, T., 2006, "Resonant Transmission in Stop Bands of Acoustic Waves in Periodic Structures," Ultrasonics, **44**(1), pp. 899–904.
[3] Hussein, M. I., Hulbert, G. M., and Scott, R. A., 2006, "Dispersive Elastodynamics of 1D Banded Materials and Structures: Analysis," J. Sound Vib., **289**(4–5), pp. 779–806.
[4] Jensen, J. S., and Pedersen, N. L., 2006, "On Maximal Eigenfrequency Separation in Two-Material Structures: The 1D and 2D Scalar Cases," J. Sound Vib., **289**(4–5), pp. 967–986.
[5] Lee, C. Y., Leamy, M. J., and Nadler, J. H., 2010, "Frequency Band Structure and Absorption Predictions for Multi-Periodic Acoustic Composites," J. Sound Vib., **329**(10), pp. 1809–1822.
[6] Aly, A. H., Mehaney, A., and Abdel-Rahman, E., 2013, "Study of Physical Parameters on the Properties of Phononic Band Gaps," Int. J. Mod. Phys. B, **27**(11), p. 1350047.
[7] Ponge, M. F., Jacob, X., and Gibiat, V., 2014, "Comparison of the Transmission Properties of Self-Similar, Periodic, and Random Multilayers at Normal Incidence," J. Acoust. Soc. Am., **135**(6), pp. 3390–3397.
[8] Nemat-Nasser, S., Sadeghia, H., Amirkhizib, A. V., and Srivastavac, A., 2015, "Phononic Layered Composites for Stress-Wave Attenuation," Mech. Res. Commun., **68**, pp. 65–69.
[9] Nemat-Nasser, S., and Srivastava, A., 2011, "Negative Effective Dynamic Mass-Density and Stiffness: Micro-Architecture and Phononic Transport in Periodic Composites," AIP Adv., **1**(4), p. 041502.
[10] Zhu, R., Huang, G. L., and Hu, G. K., 2012, "Effective Dynamic Properties and Multi-Resonant Design of Acoustic Metamaterials," ASME J. Vib. Acoust., **134**(3), p. 031006.
[11] Wang, Y., Song, W., Sun, E., Zhang, R., and Cao, W., 2014, "Tunable Passband in One-Dimensional Phononic Crystal Containing a Piezoelectric $0.62Pb(Mg_{1/3}Nb_{2/3})O_3$-$0.38\ PbTiO_3$ Single Crystal Defect Layer," Physica E, **60**, pp. 37–41.
[12] Lee, S. M., Cahill, D. G., and Venkatasubramanian, R., 1997, "Thermal Conductivity of Si-Ge Superlattices," Appl. Phys. Lett., **70**(22), pp. 2957–2959.
[13] Pernot, G., Stoffel, M., Savic, I., Pezzoli, F., Chen, P., Savelli, G., Jacquot, A., Schumann, J., Denker, U., Monch, I., Deneke, C., Schmidt, O. G., Rampnoux, J. M., Wang, S., Plissonnier, M., Rastelli, A., Dilhaire, S., and Mingo, N., 2010, "Precise Control of Thermal Conductivity at the Nanoscale Through Individual Phonon-Scattering Barriers," Nat. Mater., **9**(6), pp. 491–495.
[14] Liang, B., Guo, X. S., Tu, J., Zhang, D., and Cheng, J. C., 2010, "An Acoustic Rectifier," Nat. Mater., **9**(12), pp. 989–992.
[15] Ma, C., Parker, R. G., and Yellen, B. B., 2013, "Optimization of an Acoustic Rectifier for Uni-Directional Wave Propagation in Periodic Mass-Spring Lattices," J. Sound Vib., **332**(20), pp. 4876–4894.
[16] Saini, G., Pezeril, T., Torchinsky, D. H., Yoon, J., Kooi, S. E., Thomas, E. L., and Nelson, K. A., 2011, "Pulsed Laser Characterization of Multicomponent Polymer Acoustic and Mechanical Properties in the Sub-GHz Regime," J. Mater. Res., **22**(3), pp. 719–723.
[17] Lee, E. H., and Yang, H. W., 1973, "On Waves in Composite Materials With Periodic Structure," Soc. Ind. Appl. Math., **25**(3), pp. 492–499.
[18] He, J. J., Djafarirouhani, B., and Sapriel, J., 1988, "Theory of Light-Scattering by Longitudinal-Acoustic Phonons in Superlattices," Phys. Rev. B, **37**(8), pp. 4086–4098.
[19] Tamura, S., and Wolfe, J. P., 1988, "Acoustic Phonons in Multiconstituent Superlattices," Phys. Rev. B, **38**(8), pp. 5610–5614.
[20] Esquivel Sirvent, R., and Cocoletzi, G. H., 1994, "Band Structure for the Propagation of Elastic Waves in Superlattices," J. Acoust. Soc. Am., **95**(1), pp. 86–90.
[21] Rouhani, B. D., Dobrzynski, L., Duparc, O., Camley, R., and Maradudin, A., 1983, "Sagittal Elastic Waves in Infinite and Semi-Infinite Superlattices," Phys. Rev. B, **28**(4), pp. 1711–1720.
[22] Nougaoui, A., and Rouhani, B. D., 1987, "Elastic Waves in Periodically Layered Infinite and Semi-Infinite Anisotropic Media," Surf. Sci., **185**(1–2), pp. 125–153.
[23] Nougaoui, A., and Rouhani, B. D., 1988, "Complex Band Structure of Acoustic Waves in Superlattices," Surf. Sci., **199**(3), pp. 623–637.
[24] Sapriel, J., and Rouhani, B. D., 1989, "Vibrations in Superlattice," Surf. Sci. Rep., **10**(4–5), pp. 189–275.
[25] Nayfeh, A. H., 1991, "The General Problem of Elastic Wave Propagation in Multilayered Anisotropic Media," J. Acoust. Soc. Am., **89**(4), pp. 1521–1531.
[26] Braga, A. M. B., and Herrmann, G., 1992, "Floquet Waves in Anisotropic Periodically Layered Composites," J. Acoust. Soc. Am., **91**(3), pp. 1211–1227.
[27] Haque, A. B. M. T., and Shim, J., 2016, "On Spatial Aliasing in the Phononic Band-Structure of Layered Composites," Int. J. Solids Struct., **96**(1), pp. 380–392.
[28] Haque, A. B. M. T., Ghachi, R. F., Alnahhal, W. I., Aref, A., and Shim, J., 2017, "Generalized Spatial Aliasing Solution for the Dispersion Analysis of Infinitely Periodic Multilayered Composites Using the Finite Element Method," ASME J. Vib. Acoust., **139**(5), p. 051010.
[29] Tamura, S., and Wolfe, J. P., 1987, "Coupled-Mode Stop Bands of Acoustic Phonons in Semiconductor Superlattices," Phys. Rev. B, **35**(5), pp. 2528–2531.
[30] Hurley, D. C., Tamura, S., Wolfe, J. P., and Morkoc, H., 1987, "Imaging of Acoustic Phonon Stop Bands in Superlattices," Phys. Rev. Lett., **58**(23), pp. 2446–2449.
[31] Calle, F., and Cardona, M., 1989, "Frequency Gaps for Folded Acoustic Phonons in Superlattices," Solid State Commun., **72**(12), pp. 1153–1158.
[32] Mizuno, S., 2003, "Resonance and Mode Conversion of Phonons Scattered by Superlattices With Inhomogeneity," Phys. Rev. B, **68**(19), p. 193305.
[33] Pennec, Y., Djafari-Rouhani, B., Larabi, H., Vasseur, J. O., and Hladky-Hennion, A. C., 2008, "Low-Frequency Gaps in a Phononic Crystal Constituted of Cylindrical Dots Deposited on a Thin Homogeneous Plate," Phys. Rev. B, **78**(10), p. 104105.
[34] Assouar, M. B., Senesi, M., Oudich, M., Ruzzene, M., and Hou, Z. L., 2012, "Broadband Plate-Type Acoustic Metamaterial for Low-Frequency Sound Attenuation," Appl. Phys. Lett., **101**(17), p. 173505.
[35] Varanasi, S., Bolton, J. S., Siegmund, T. H., and Cipra, R. J., 2013, "The Low Frequency Performance of Metamaterial Barriers Based on Cellular Structures," Appl. Acoust., **74**(4), pp. 485–495.
[36] Hayashi, T., Morimoto, Y., Serikawa, M., Tokuda, K., and Tanaka, T., 1983, "Experimental Study on Cut-Off Phenomenon for Layered Composite," Bull. JSME, **26**(211), pp. 23–29.
[37] Marechal, P., Lenoir, O., Khaled, A., El Kettani, M. E. C., and Chenouni, D., 2014, "Viscoelasticity Effect on a Periodic Plane Medium Immersed in Water," Acta Acust. Acust., **100**(6), pp. 1036–1043.
[38] Tanaka, K., and Kon-No, A., 1980, "Harmonic Viscoelastic Waves Propagating Normal to the Layers of Laminated Media," Bull. JSME, **23**(181), pp. 1092–1099.
[39] Mukherjee, S., and Lee, E. H., 1975, "Dispersion Relations and Mode Shapes for Waves in Laminated Viscoelastic Composites by Finite Difference Methods," Comput. Struct., **5**(5–6), pp. 279–285.

[40] Mukherjee, S., and Lee, E., 1978, "Dispersion Relations and Mode Shapes for Waves in Laminated Viscoelastic Composites by Variational Methods," Int. J. Solids Struct., **14**(1), pp. 1–13.
[41] Chevalier, Y., 1988, "Dispersion of Harmonic Waves in Elastic and Viscoelastic Periodic Composite Materials," *Recent Developments in Surface Acoustic Waves: Proceedings of European Mechanics Colloquium*, Vol. 7, D. F. Parker, and G. A. Maugin, eds., Springer, Berlin, pp. 260–268.
[42] Zhao, Y. P., and Wei, P. J., 2009, "The Band Gap of 1D Viscoelastic Phononic Crystal," Comput. Mater. Sci., **46**(3), pp. 603–606.
[43] Cooper, H. F., and Reiss, E. L., 1966, "Reflection of Plane Viscoelastic Waves From Plane Boundaries," J. Acoust. Soc. Am., **39**(6), pp. 1133–1138.
[44] Shaw, R. P., and Bugl, P., 1969, "Transmission of Plane Waves Through Layered Linear Viscoelastic Media," J. Acoust. Soc. Am., **46**(3), pp. 649–654.
[45] Borcherdt, R. D., 2009, *Viscoelastic Waves in Layered Media*, Cambridge University Press, Cambridge, UK.
[46] Schoenberg, M., 1971, "Transmission and Reflection of Plane Waves at an Elastic-Viscoelastic Interface," Geophys. J. R. Astron. Soc., **25**(1–3), pp. 35–47.
[47] Silva, W., 1976, "Body Waves in a Layered Anelastic Solid," Bull. Seismol. Soc. Am., **66**(5), pp. 1539–1554.
[48] Borcherdt, R. D., 1977, "Reflection and Refraction of Type-II S Waves in Elastic and Anelastic Media," Bull. Seismol. Soc. Am., **67**(1), pp. 43–67.
[49] Borcherdt, R. D., 1982, "Reflection-Refraction of General P- and Type-I S-Waves in Elastic and Anelastic Solids," Geophys. J. R. Astron. Soc., **70**(3), pp. 621–638.
[50] Krebes, E. S., 1983, "The Viscoelastic Reflection/Transmission Problem: Two Special Cases," Bull. Seismol. Soc. Am., **73**(6), pp. 1673–1683.
[51] Borcherdt, R. D., and Wennerberg, L., 1985, "General P, Type-I S and Type-II S Waves in Anelastic Solids; Inhomogeneous Wave Fields in Low-Loss Solids," Bull. Seismol. Soc. Am., **75**(6), pp. 1729–1763.
[52] Sharma, M. D., 2015, "Snell's Law at the Boundaries of Real Elastic Media," Math. Stud., **84**(3–4), pp. 75–94.
[53] Sharma, M. D., 2011, "Wave Propagation in a Dissipative Poroelastic Medium," IMA J. Appl. Math., **78**(1), pp. 59–69.
[54] Buchen, P. W., 1971, "Plane Waves in Linear Viscoelastic Media," Geophys. J. R. Astron. Soc., **23**(5), pp. 531–542.
[55] Borcherdt, R. D., 1973, "Energy and Plane Waves in Linear Viscoelastic Media," J. Geophys. Res., **78**(14), pp. 2442–2453.
[56] Brinson, H. F., and Brinson, L. C., 2008, *Polymer Engineering Science and Viscoelasticity: An Introduction*, Springer, New York.
[57] Banergee, B., 2011, *An Introduction to Metamaterials and Waves in Composites*, CRC Press, Boca Raton, FL.
[58] Coquin, G., 1964, "Attenuation of Guided Waves in Isotropic Viscoelastic Materials," J. Acoust. Soc. Am., **36**(6), pp. 1074–1080.
[59] Garcia-Barruetabena, J., Cortes, F., Manuel Abete, J., Fernandez, P., Jesus Lamela, M., and Fernandez-Canteli, A., 2013, "Relaxation Modulus-Complex Modulus Interconversion for Linear Viscoelastic Materials," Mech. Time-Depend. Mater., **17**(3), pp. 465–479.
[60] Pike, R., and Sabatier, P., 2002, *Scattering: Scattering and Inverse Scattering in Pure and Applied Science*, Academic Press, London.
[61] Lockett, F. J., 1962, "The Reflection and Refraction of Waves at an Interface Between Viscoelastic Materials," J. Mech. Phys. Solids, **10**(1), pp. 53–64.
[62] Cooper, H. F., 1967, "Reflection and Transmission of Oblique Plane Waves at a Plane Interface Between Viscoelastic Media," J. Acoust. Soc. Am., **42**(5), pp. 1064–1069.
[63] Sharma, M. D., and Vashishth, A. K., 2011, "Intrinsic Attenuation From Inhomogeneous Waves in a Dissipative Anisotropic Poroelastic Medium," Earth, Planets Space, **63**(2), pp. 89–101.
[64] Graff, K. F., 1991, *Wave Motion in Elastic Solids*, Dover Publications, Mineola, NY.
[65] Kittel, C., 2004, *Introduction to Solid State Physics*, 8th ed., Wiley, New York.
[66] Ashcroft, N. W., and Mermin, N. D., 1976, *Solid State Physics*, Saunders College, Philadelphia, PA.
[67] Birkhoff, G., and MacLane, S., 1977, *A Survey of Modern Algebra*, 4th ed., Macmillan Publishing, New York.
[68] Jensen, F. B., Schmidt, H., Porter, M. B., and Kuperman, W. A., 2011, *Computational Ocean Acoustics*, Springer, New York.
[69] Brito-Santana, H., Wang, Y. S., Rodriguez-Ramos, R., Bravo-Castillero, J., Guinovart-Diaz, R., and Tita, V., 2015, "A Dispersive Nonlocal Model for In-Plane Wave Propagation in Laminated Composites With Periodic Structures," ASME J. Appl. Mech., **82**(3), p. 031006.
[70] Brito-Santana, H., Wang, Y. S., Rodriguez-Ramos, R., Bravo-Castillero, J., Guinovart-Diaz, R., and Tita, V., 2015, "A Dispersive Nonlocal Model for Shear Wave Propagation in Laminated Composites With Periodic Structures," Eur. J. Mech. A, **49**(1), pp. 35–48.
[71] Theocharis, G., Richoux, O., Garcia, V. R., Merkel, A., and Tournat, V., 2014, "Limits of Slow Sound Propagation and Transparency in Lossy, Locally Resonant Periodic Structures," New J. Phys., **16**(1), p. 093017.
[72] Yu, G. K., and Wang, X. L., 2014, "Acoustical 'Transparency' Induced by Local Resonance in Bragg Bandgaps," J. Appl. Phys., **115**(4), p. 044913.
[73] Groby, J. P., Huang, W., Lardeau, A., and Auregan, Y., 2015, "The Use of Slow Waves to Design Simple Sound Absorbing Materials," J. Appl. Phys., **117**(12), p. 124903.
[74] Groby, J. P., Pommier, R., and Auregan, Y., 2016, "Use of Slow Sound to Design Perfect and Broadband Passive Sound Absorbing Materials," J. Acoust. Soc. Am., **139**(4), pp. 1660–1671.
[75] Potel, C., and de Belleval, J. F., 1993, "Propagation in an Anisotropic Periodically Multilayered Medium," J. Acoust. Soc. Am., **93**(5), pp. 2669–2677.
[76] Sigalas, M. M., and Soukoulis, C. M., 1995, "Elastic-Wave Propagation Through Disordered and/or Absorptive Layered Systems," Phys. Rev. B, **51**(5), pp. 2780–2789.
[77] Bousfia, A., El Boudouti, E. H., Djafari-Rouhani, B., Bria, D., Nougaoui, A., and Velasco, V. R., 2001, "Omnidirectional Phononic Reflection and Selective Transmission in One-Dimensional Acoustic Layered Structures," Surf. Sci., **482–485**(2), pp. 1175–1180.
[78] Bria, D., Djafari-Rouhani, B., Bousfia, A., El Boudouti, E. H., and Nougaoui, A., 2001, "Absolute Acoustic Band Gap in Coupled Multilayer Structures," Europhys. Lett., **55**(6), pp. 841–846.
[79] Shen, M. R., and Cao, W. W., 1999, "Acoustic Band-Gap Engineering Using Finite-Size Layered Structures of Multiple Periodicity," Appl. Phys. Lett., **75**(23), pp. 3713–3715.
[80] Shen, M. R., and Cao, W. W., 2000, "Acoustic Bandgap Formation in a Periodic Structure With Multilayer Unit Cells," J. Phys. D: Appl. Phys., **33**(10), pp. 1150–1154.
[81] Santos, P. V., Mebert, J., Koblinger, O., and Ley, L., 1987, "Experimental Evidence for Coupled-Mode Phonon Gaps in Superlattice Structures," Phys. Rev. B, **36**(2), pp. 1306–1309.
[82] Naciri, T., Navi, P., and Granacher, O., 1990, "On Harmonic Wave Propagation in Multilayered Viscoelastic Media," Int. J. Mech. Sci., **32**(3), pp. 225–231.